Atomic Control in Multicomponent Nanomaterials: when Colloidal Chemistry meets Atomic Layer Deposition

Anna Loiudice[+], Ona Segura[+], Raffaella Buonsanti*

Laboratory of Nanochemistry for Energy (LNCE), Department of Chemical Sciences and Engineering, École Polytechnique Fédérale de Lausanne, CH-1950 Sion, Switzerland.

+ Equal contribution

Abstract

In the past decades, atomically controlled multicomponent nanomaterials have served as platforms to advance the understanding of scientific phenomena along with providing practical solutions for various applications. Colloidal chemistry and atomic layer deposition techniques are two of the most powerful techniques to tailor make materials with tunable composition and morphology. In this review we focus on how the combination of these two highly versatile chemistries enables an exquisite control at the atomic scale of multicomponent nanomaterials in a wide compositional range. We discuss very recent studies from us and others, which encourage the scientific community to explore the tunability offered by such combination even further.

1. Introduction

Atomically-controlled multicomponent nanomaterials have advanced the understanding of scientific phenomena and devised solutions to practical problems, enabling technological progress in many application fields.[1,2] Their properties are strongly influenced by composition, geometries and interfaces between the constituent building blocks, as new and unpredictable functionalities can emerge from the intimate

contact between highly contrastingly materials. Thus, developing the chemistry to fine tune these physical parameters is of the uttermost importance.

In this contribution, we discuss the recent progress in multicomponent nanomaterials comprising colloidally-synthesized nanocrystals (NCs) and a matrix prepared by atomic layer deposition (ALD).

On one end, colloidal chemistry is one of the most powerful wet-chemistry techniques to obtain monodisperse particles with size ranging from 10^{-7} to 10^{-9} m and controllable shape suspended in a dispersing medium forming a colloidal solution.[3,4] Wet-chemical methods are bottom-up strategies that allow one to obtain zero, one and two-dimensional nanomaterials, a degree of freedom not always granted by top-down approaches.[5]

On the other, ALD is one of the best techniques to synthesize nanometer-thin conformal layers. This approach is based on sequential and self-limited half-reactions: the precursors are never present simultaneously in the reactor, as they are inserted in non-overlapping pulses, and the precursor molecules of these pulses react with the surface in a self-terminating way, so that the reaction is completed once all the reactive sites on the surface are consumed.[6]

In this review, we highlight how the combination of these two highly versatile chemistries enables an exquisite control at the atomic scale of multicomponent nanomaterials in a wide compositional range, including dielectrics, semiconductors and metals. In addition to the traditional gas-phase ALD performed in a vacuum chamber, we include the emerging colloidal ALD in solution phase (c-ALD). While less developed in the understanding of the chemistry behind it, c-ALD is attracting increasing interest in the scientific community as it offers the unique opportunities of the layer-by-layer growth of the gas-phase ALD but in solvents, thus facilitating post-

synthetic material processability. Colloidal NC films infilled with a matrix deposited by gas-phase ALD will be referred to as nanocomposites. Instead, the multicomponent nanomaterials obtained by coating colloidal NCs with c-ALD grown shell will be indicated as core@shell NC heterostructures. Along with reviewing the literature, we will elaborate on some of the open challenges, before concluding with an outlook on future opportunities offered by the combination of these two powerful synthesis techniques.

2. General principles of the synthetic techniques

2.1 Colloidal synthesis of nanocrystals

Colloidal synthesis is a wet-chemistry surfactant-assisted approach that is among the most versatile technique for nanoscale material synthesis. First, it enables a wide compositional and morphological tunability of the NCs. Secondly, it offers the possibility to obtain unsupported colloidally stable NCs that can be then easily processed, for example deposited onto various substrates by different techniques (i.e. spin-coating, drop casting, doctor blade, etc.) or integrated into various matrices (i.e. by mixing in compatible solvents).[7,8] These two features are hardly simultaneously accessible by physical nanostructuring techniques such as electron or molecular beam lithography. For these reasons, synthetic efforts have been dedicated towards a variety of metals, metal oxides, and semiconductors which have been developed in the form of size- and shape-controlled NCs via colloidal chemistry.[9,10] The achieved degree of control enables tunability and control on the optical, magnetic, catalytic properties which are dependent by these structural parameters.

A typical colloidal synthesis employs metal salts as precursors, often a reducing agent, organic ligands (or surfactants) and a carrier solvent that are mixed together in a three-

neck reaction flask connected to a Schlenk-line. The NC size and shape are sensitive to several parameters, including temperature (ranging between room temperature and 400 ºC), reaction duration, overall concentrations as well as the time and rate of injection of additional reactants.[11,12] Surfactants are crucial as they play several roles during the synthesis. First, they may react with the metal salts and form the monomeric species (i.e. molecular complexes or clusters), which are responsible for the initial step of the NC nucleation.[13] Simultaneously, they define the NC size by participating in adsorption/desorption dynamic processes on the surface of the growing nuclei preventing their aggregation and uncontrolled growth. Finally, surfactants can affect the specific surface energy of the growing NCs, which has implications in the tuning of their shape.[11,14,15] Indeed, facet-preferential ligand adhesion can modify the relative growth rates along the various crystallographic directions and/or can favor selective elimination of unstable surfaces by triggering oriented attachment of particles along defined crystallographic directions. This mechanism remains responsible for most of the NC formation in a variety of anisotropic shapes, such as cubes, polyhedrons, rods, wires, polypods, etc.. Surfactants remain on the NC surface after the synthesis granting their colloidal stability in aqueous or organic solvents depending from their polarity. Various exchange procedures have been developed to substitute the original ligands used during the synthesis with new ligands possessing different functionalities designed according to the desired surface properties. Finally, ligands have also been regarded as a tool to engineer the NC self-assembly capabilities.[16–19]

The NC complexity accessible by colloidal chemistry is rapidly expanding, in terms of both shape engineering and compositional variety. Many studies have recently shown how carefully control on the NC shape is advantageous and essential to investigate structure/properties relationship in various areas of application.[20–22] To give one

example, copper NCs with different sizes and shapes (**Figure 1a**) have been used to study and optimize facet-dependent selectivity in a conversion process very relevant for sustainability, which is the electrochemical CO_2 reduction (**Figure 1b**).[21,23–26]

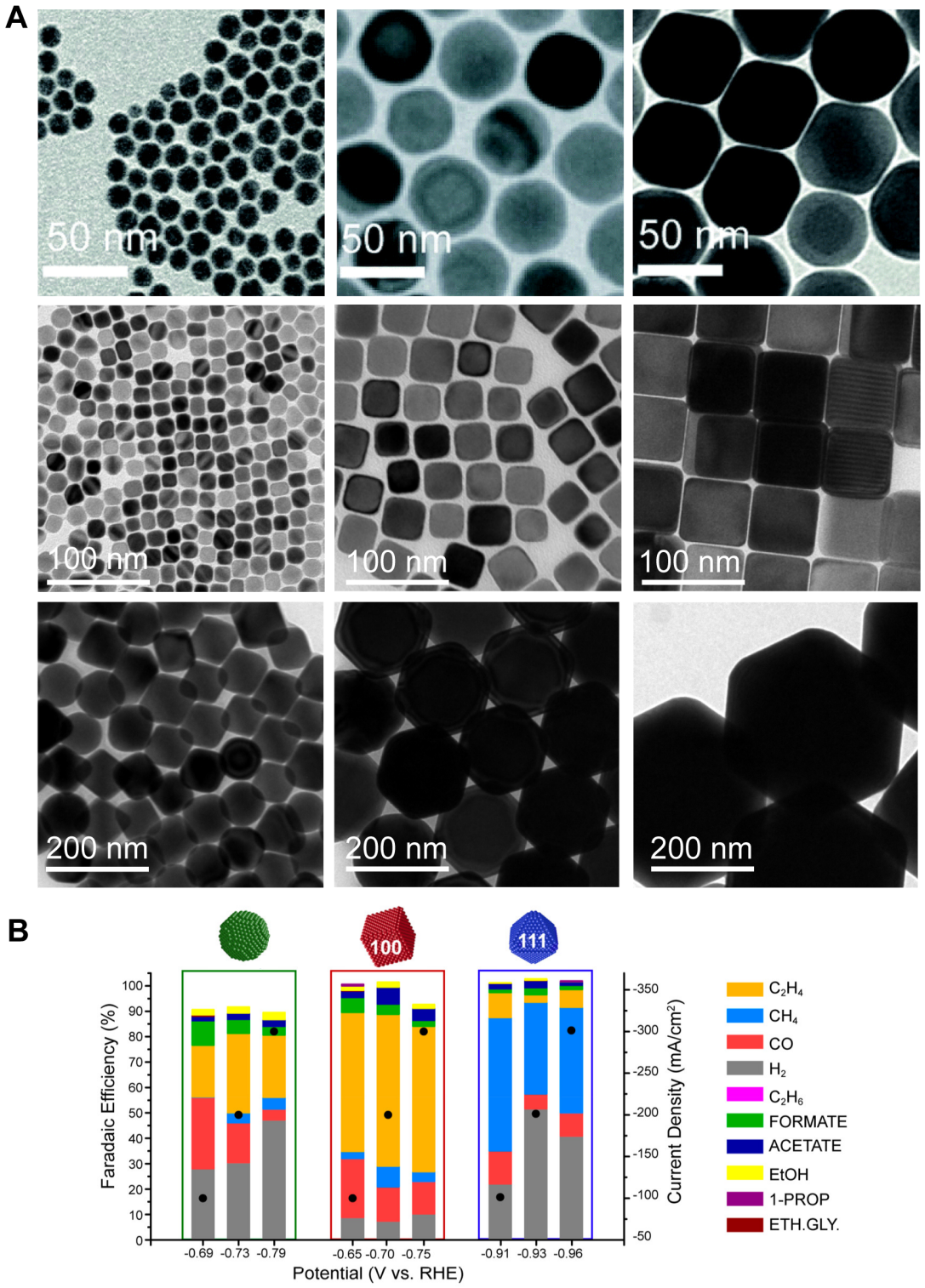

Figure 1. a) Transmission electron microscopy (TEM) images of spherical, cubic and octahedral copper NCs of different sizes, reprinted with permission from ref. (25) and (26). Copyright 2018 The Royal Society of Chemistry. Copyright 2018 Nature

Publishing Group. b) Faradaic efficiencies for the electrochemical CO_2 reduction reaction using copper sphere, cubes and octahedra as catalysts. These measurements were performed in a gas-fed flow cell at commercially viable current densities and potential. Reprinted with permission from ref. (24). Copyright 2020 American Chemical Society.

At present, much research focuses on solving challenges in the synthesis of novel NCs, such as highly covalent group IV elements (Si, Ge), III-V compounds (GaAs, InAs, InSb, etc.), multicomponent chalcogenides and metal oxides (Cu_3VS_4, $CuInS_2$, $BiVO_4$, Cu_3PS_4, Fe_2GeS_4, etc.), or carbon-based compositions.[25,27–37] Moreover continuing efforts are underway to engineer NC composition and morphology by means of galvanic replacement, ion-exchange reactions, or through the nanoscale Kirkendall effect.[38–40] Finally, another emerging area is the development of in-situ characterization methods to obtain insights into the nucleation and growth of NCs or to monitor the structural and compositional evolution of the NCs during operation in various devices.[15,41–44]

2.2 Gas-phase ALD

ALD is a vapor-phase deposition technique that occurs through sequential self-limiting surface reactions and was first developed in the 1970s by Suntola and Antson for ZnS growth.[45] During the following years, the use of ALD expanded tremendously to growth a variety of materials that include metals, metal oxides, alloys and nanolaminates making this technique appealing for many areas of applications such as energy technologies, like photovoltaic, catalysis and batteries, or micro and nanoelectronics.[46–49]

The ALD process is illustrated in **Figure 2**. Here, the growth cycle for a thin film of a binary metal oxide (Al_2O_3) from gaseous precursors (Trimethyl aluminum (TMA) and water (H_2O)) is presented as one example. In the first step, one of the precursors is pulsed into the reactor (a vacuum chamber) and reacts onto the surface of the substrate

through a self-limiting process that leaves no more than one monolayer at the surface; after reaching saturation, the excess reactant is purged with an inert gas. The co-reactant is then introduced in the system and reacts with the precursor already adsorbed on the surface. Again, the chemistry is chosen such that this step is self-limiting, causing the surface reaction to cease after no more than one monolayer coverage. Finally, the excess co-reactant is purged from the system, creating the first monolayer of the targeted material. This process is repeated in a layer-by-layer fashion until the desired thickness is achieved.

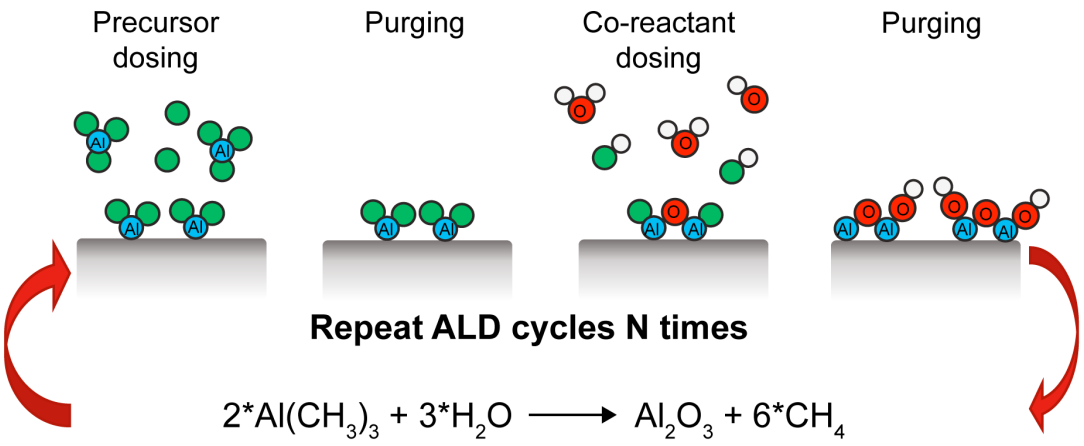

Figure 2. Representative scheme of a standard thermal ALD process.

The primary advantages of ALD are all derived from the sequential, self-saturating, gas-surface reaction control of the deposition process. Firstly, the conformality of ALD-deposited films is often the critical factor in choosing ALD over competing deposition techniques, such as chemical or physical vapor deposition (CVD and PVD) and sputtering, or solution-based techniques, such as sol-gel.[50–52] Conformality of high aspect ratio and porous/tortuous materials is made possible by its self-limiting characteristic, which restricts the reaction at the surface to no more than a monolayer of precursor. Subsequent cycles allow for uniform growth even on high aspect ratio and porous structures, whereas CVD or other techniques may suffer from non-uniformity

due to faster surface reactions and shadowing effects, respectively. A second advantage is the sub-nanometer thickness control that could be tailored by the number of ALD cycles.

Different parameters control the ALD process, including chamber temperature and pressure, duration of precursors pulses and waiting times between one pulse and the other, that all together will define the growth per cycle (GPC) of the process. Between those, temperature plays an important role. In order to benefit from the many advantages of ALD, it is desirable to operate within the designated optimal ALD temperature window, which is moderately elevated (<350ºC). Temperatures outside of the window generally result in poor GPC and non-ALD type deposition due to effects such as slow reaction kinetics or precursor adsorption (at low temperature) and thermal decomposition or rapid desorption of the precursor (at high temperature).

The first step in an ALD process is the nucleation that is extremely important for continuous and pinhole-free ultrathin films. The nucleation strongly depends from the reactivity of the precursors with the substrate surface. If the ALD precursors do not effectively react with the initial substrate, then the ALD film may not form at all or may form only at particular defect sites on the surface.[53] Improvements of the uniformity might be achieved via surface treatments and functionalizations.[54]

In general, two main disadvantages can be listed for the ALD techniques. First, it is a much slower process compared to other techniques, as the grow rate is in the range of 100-300 nm/hour. Second, the high temperatures required to make certain precursor reactive enough with the surface may be incompatible with certain substrates or materials. Nevertheless, ALD assisted by UV-light or plasma could help to widen the chemical species which can be suitable as precursors during the process.[53,55]

2.3 Colloidal ALD

Following the development of gas-phase ALD, the successive ionic layer absorption and reaction (SILAR) technique was introduced as a way to extend the ALD principles to the growth of thin films in solution. Here, the substrates are sequentially immersed into the precursor and co-reactant baths, typically aqueous solutions of metal salts and salts, and washed with suitable solvents in between to eliminate the reagents excess.[56,57,58] Using this technique, binary composites such as metal oxides and chalcogenides, as well as ternary (Cu-Sn-S) and quaternary (Cu_2ZnSnS_4 or $Cu_2ZnSnSe_4$) compounds have been deposited and used for solar energy harvesting applications, gas sensors, LED and supercapacitors.[59–64,65–72] As the process is carried out at or near room temperature, a great variety of substrates has been used, including polymeric materials.[61]

From the growth of thin films in solution, SILAR has then been extended as a post-synthetic treatment to modify the surface of semiconductor NCs both deposited in films and dispersed in solution; the latter has been referred to as colloidal SILAR (c-SILAR).[73–77] To cite one example, Treml et al. applied the SILAR method to grow a homogeneous (PbSe) or heterogeneous (CdSe) coating on PbSe quantum dots (QDs) assembled in thin films in order to enhance the interdot bonds and thus to strengthen the electronic interactions.[73] As for c-SILAR, CdSe@CdS core@shell QDs were first prepared by Peng and co-workers, but many others have then followed the same procedure to grow multilayered and multicomponent shells on QD cores (i.e. CdSe@$Zn_xCd_{1-x}S$, CdSe@ZnS, InP@CdS).[75,78–81] One of the major drawbacks with c-SILAR is that the reaction involved is not self-limiting. Because too many assumptions are made when calculating the amount of the precursor to add (i.e. all the NC surface active sites), unreacted precursor can still remain in solution and induce homogeneous

nucleation of semiconductor seeds, or, contrarily, it might not be sufficient to cover the whole NC surface.[76]

In 2012 the concept of c-ALD was finally introduced by Ithurria et al., thus enabling to overcome this issue.[82] The authors proposed a biphasic reaction where the NCs are dispersed in a non-polar liquid phase and the precursors for the shell growth are solubilized in a polar solvent. Vigorous agitation allows mixing of the phases and reaction of the precursors on the NC surface. The non-miscibility of the phases allow the excess reagents to be rapidly removed. This approach has been so far utilized only for chalcogenides

Recently, an alternative c-ALD method has been proposed for the growth of oxide shells. Here, the process occurs in a reaction vessel where the NCs are dispersed in solution and the reagents for the shell, either liquid or gas, are introduced dropwise in an alternating fashion.[83,84] Le Monnier et al. have developed a liquid-phase ALD where previous titration of the surface reactive sites allows for stoichiometrically limited injections of the precursor (metal alkoxides) and co-reactant (H_2O).[83] An alternative methodology has been proposed by Loiudice et al. where pure oxygen is employed as the co-reactant; the gaseous nature of the precursor facilitates in great measure the purging step and also enables the extension to core materials sensitive to water.[84]

Overall, **Figure 3** compares these two c-ALD methodologies (**Figure 3a,b**) to the more conventional gas-phase ALD (**Figure 3c**) highlighting the similarities.

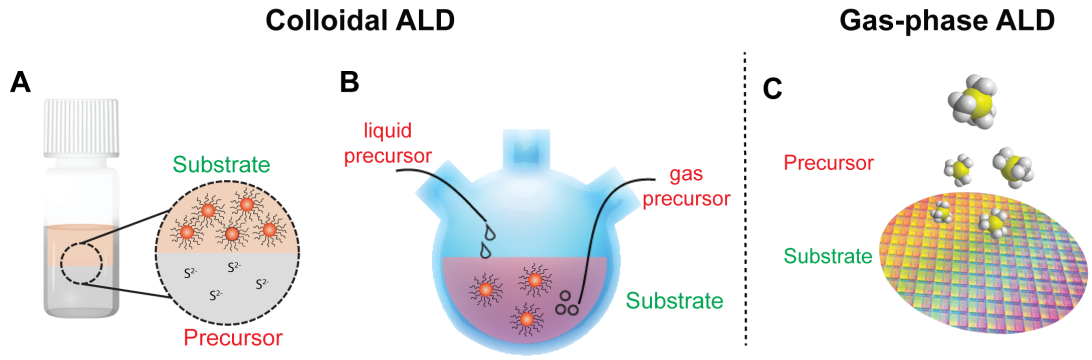

Figure 3. Schematic comparing the colloidal ALD approaches (a,b) with the gas-phase ALD (c).

3. Nanocomposites by coating NC films with an ALD matrix

3.1 State-of-the-art for the synthesis

Up to date most of the studies reporting on the synthesis of nanocomposite by ALD in film include the use of colloidal QDs as the nanocomponent. Nanocomposite with varied compositions have been reported including CdSe, CdSe/CdS/ZnS, PbS, PbSe QDs and, more recently, the highly sensitive perovskite $CsPbX_3$ (X=Br,Cl and I) and InP QDs, as the nanocomponent, while mostly metal oxide, such as Al_2O_3, ZnO or TiO_2, have been employed as the ALD matrix.

In these nanocomposites, the ALD matrix can have two purposes: 1) to serve as an electronic matrix that passivates surface states and reduces the size of the inter-QD tunnel barrier governing charge transport in QD films, and 2) to act as a gas diffusion barrier/nanoscale cement to prevent the QD oxidation and to inhibit solid-state diffusion phenomena within the films. Towards these goals, two steps are key during the synthesis: infilling, i.e. ALD matrix infiltrates the pores in between the NCs, and overcoating, i.e. a capping layer forms, respectively (**Figure 4a**).

As mentioned above, gas-phase ALD is a superior method to conformally coat highly porous structures, therefore it is ideal to infill QD films wherein the pores in between the QDs are only a few nanometers. To successfully infill QD films, particular care must be taken for the nucleation step to allow a uniform coverage of the surface by the precusor. Generally, temperature must be kept below 100°C to avoid NC sintering which occurs even more rapidly under vacuum conditions.[85] This requirement represents a challenge as often higher temperatures are needed to assure high reactivity of the precursors.

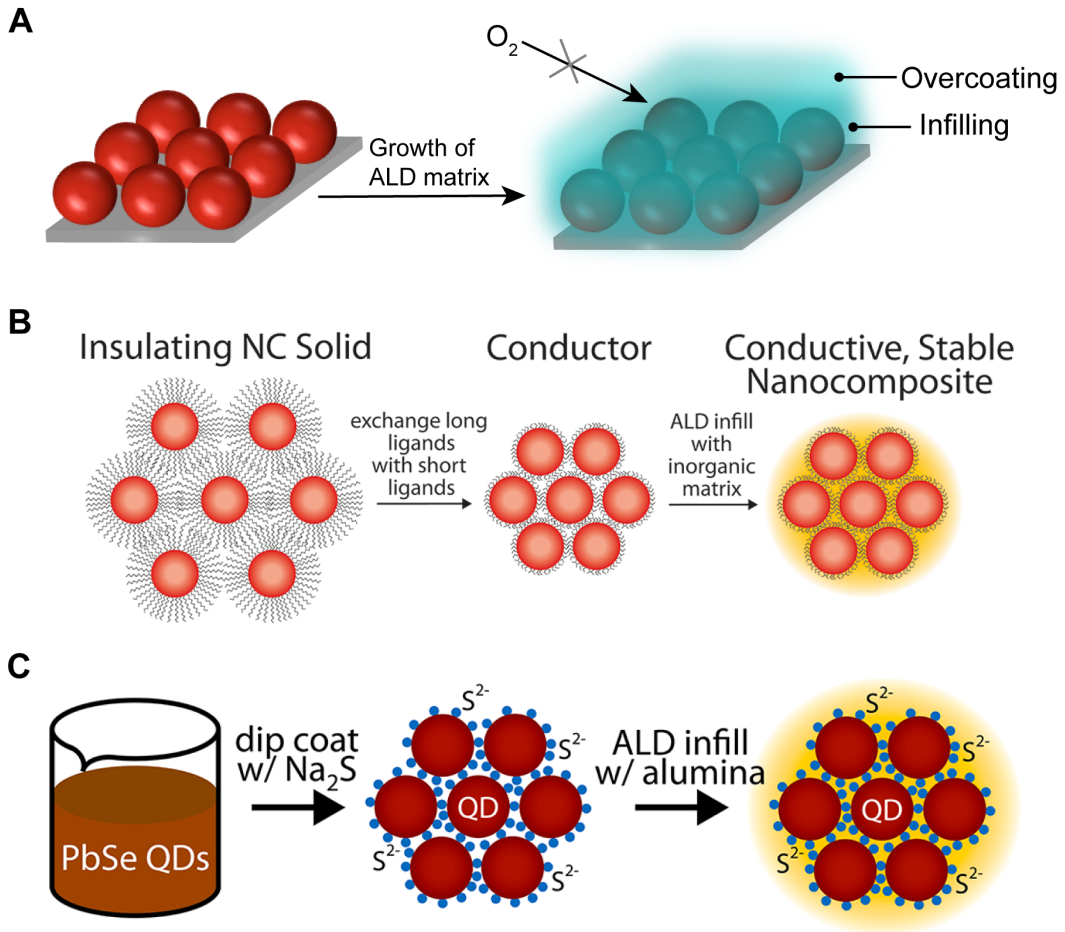

Figure 4. a) Schematic of the infilling and overcoating in nanocomposite by ALD. b) ALD infill of PbSe QDs with alumina after ligand exchange, reprinted with permission from ref. (88). Copyright 2011 American Chemical Society. c) ALD infill of sulfide-capped PbSe QDs, reprinted with permission from ref. (89). Copyright 2013 American Chemical Society.

Initial investigations on embedding QD films in an ALD matrix compared the use of thermal ALD with plasma-enhanced ALD (PE-ALD). They showed that thermal ALD is preferred to PE-ALD because it does not alter the structure or the optical absorbance properties of the QD layers.[86] For these reasons, following studies have mostly used thermal ALD for the nanocomposite synthesis. They will be described here while highlighting the effects of both infilling and overcoating.

Ihyl et al. performed one of the first studies in the field where the pores of a PbS QD film were infilled with an alumina matrix by a room temperature ALD process (**Figure 4b**).[87] The authors showed that the infilling serves as a 3D inorganic matrix to inhibit oxygen diffusion that causes PbS QDs oxidation, or ripening and sintering occurring when QD are exposed to UV-light or heating.

Later on, the same group demonstrated the advantage of exchanging the long native ligands present on PbSe QDs with short ones (**Figure 4c**) to produce inorganic nanocomposites with improved conductivity suitable for field effect transistors and solar cells with enhanced and stable performance for at least months in air.[88] Indeed, the electron mobility was increased from 1 to 7 $cm^2V^{-1}s^{-1}$ as a result of the achieved strong electronic coupling, obtained with the ligand exchange, and passivation of surface states from the ALD coating.[89] Similar results were obtained by Hu et al. for PbS/Al_2O_3 nanocomposite with S^{2-} and OH^- used as ligands.[90]

Similarly to PbSe or PbS QDs, nanocomposites containing Cd-chalcogenide QDs (CdTe, CdSe/ZnS, CdSe, CdSe/ZnS, etc.) have also been reported.[91–94] Enhanced stability under prolonged exposure to light and high temperature in ambient air has been demonstrated thanks to the presence of the ALD infilling and overcoating matrix of alumina.[91–94]

Recently ALD has been successfully applied also to highly sensitive and unstable cores such as perovskite QDs. Loiudice et al. have synthesized $CsPbX_3/AlO_x$ nanocomposite (with X=Br, I) (**Figure 5a,b**).[95] The high sensitivity to moisture, temperature, and light of this class of QDs makes the development of an optimal ALD process not trivial. In this work, it is shown that low temperature and short water pulses are mandatory to avoid QD degradation. The authors demonstrated that the infilled AlO_x matrix prevents the perovskite QDs from sintering and that the overcoating protects from oxygen and moisture conferring them stability in water (**Figure 5c**). The nucleation and growth steps of the alumina deposition process were studied in depth by combining miscellaneous techniques allowing the authors to propose the following nucleation mechanism: in the initial stage of nucleation, the aluminum precursor (TMA) reacts with the partially oxidized QD surface; upon saturation of the oxidized surface sites, the TMA molecules react with the oxygen containing ligand present on the QD surface. Finally, another example of ALD applied to highly unstable cores has been reported by Crisp et al. (**Figure 5d**). The authors grew a functional electron transport layer of either TiO_2 or ZnO via ALD on InP QDs. The envisioned functions of these ALD coatings were to (1) cause charge separation, (2) reduce recombination, (3) enhance charge transport in the film, and (4) increase stability. The authors demonstrated that the addition of ZnO coatings results in charge separation and a concomitant strong increase in photoconductivity and carrier lifetime.[96]

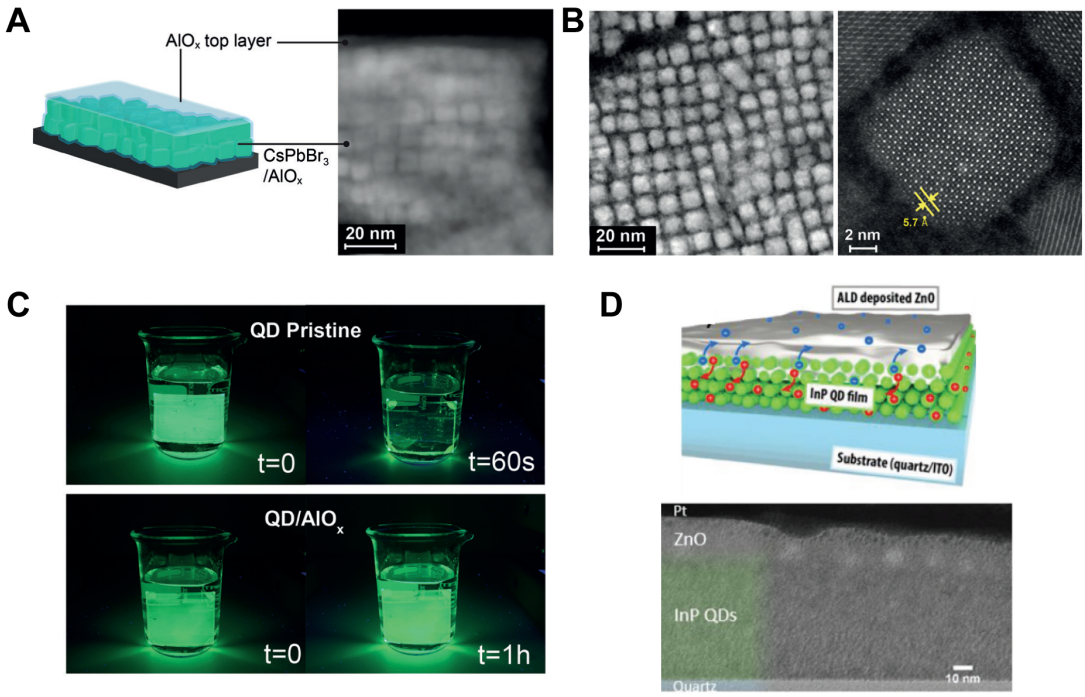

Figure 5. Nanocomposites including sensitive QDs: a) cross-sectional high angular dark field scanning transmission electron microscopy (HAADF-STEM) image of a $CsPbBr_3/AlO_x$ nanocomposite and b) top image view together with a high-resolution image. c) Photos of the nanocomposite immersed in water compared with the pristine QD film; a) b) and c) reprinted with permission from ref. (95). Copyright 2020 John Wiley and Sons. d) Cross-sectional TEM image of InP/ZnO nanocomposite together with a schematic of the same, reprinted with permission from ref. (96). Copyright 2020 John Wiley and Sons.

3.2 Characterization techniques

Because of the low dimensionality of the nanocomposite constituents, characterizing the uniformity and conformality of the ALD matrix in the NC films is not straightforward.

Depth-profiling X-ray photoelectron spectroscopy (XPS) has been widely used to assess whether infilling or only overcoating is taking place. **Figure 6a** illustrates one example of XPS elemental depth profile analysis comparing a multilayer film of 6 nm PbSe QDs infilled and overcoated with alumina deposited by ALD from trimethylaluminum and H_2O at 70 ºC. The overcoated sample was obtained by using shorter water purge times resulting in a CVD-like fashion to yield an oxide overlayer

without substantial pore filling. The main difference between the two samples is the presence of the aluminum and oxygen signal (gray line) throughout the entire QD layer up to reaching to the substrate (indium tin oxide (ITO) coated glass) in the case of the infilled nanocomposite.

Cross-section electron microscopy imaging, in particular HAADF-STEM together with elemental mapping analysis (energy dispersing X-ray spectroscopy (EDXS) or electron energy loss spectroscopy (EELS)) are complementary to XPS as they offer a higher nanometer scale resolution. Nevertheless, this technique is challenged by sample preparation. Conventional sample preparation techniques for the cross-section TEM include embedding the NC film in a resin, mechanical polishing and/or ion beam milling with a broad or focused beam; all these treatments will certainly damage nanocomposites including more sensitive NCs. Loiudice et al. had to developed a novel approach to sample preparation based on dry ultramicrotomy on a soft polymer substrate in order to demonstrate the infilling in $CsPbBr_3/AlO_x$ nanocomposite (**Figure 6b,c**).[95]

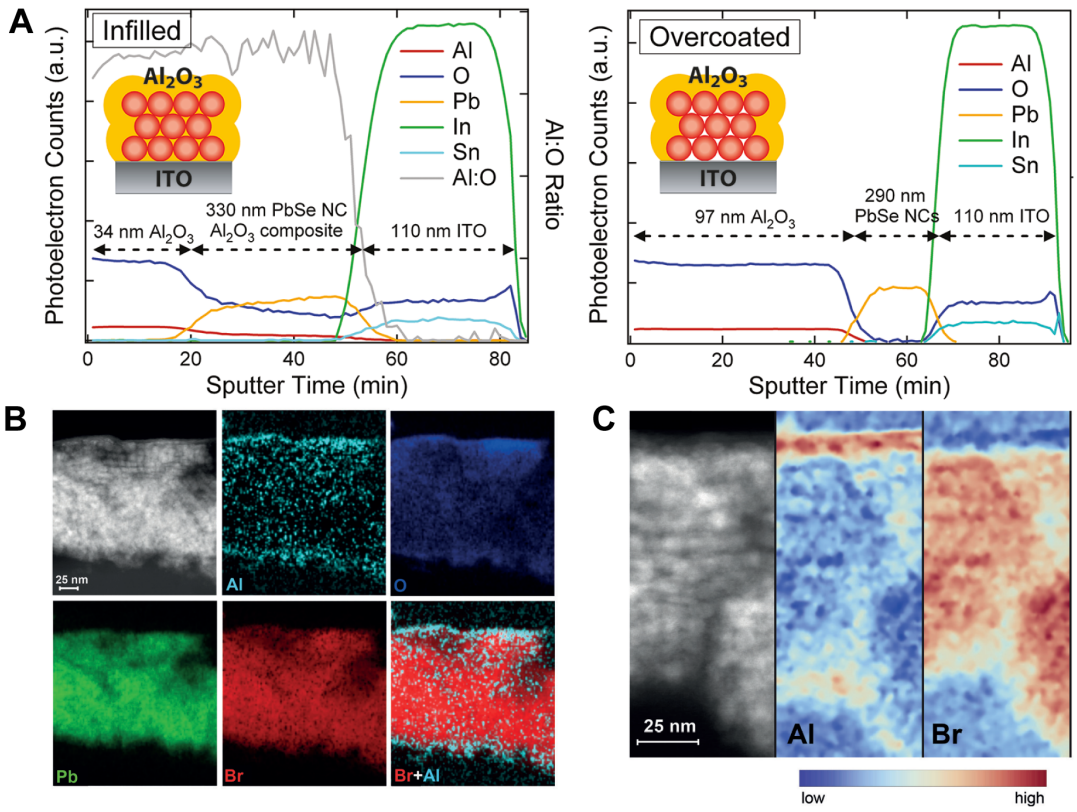

Figure 6. a) XPS depth profile of a PbSe QD film infilled (left) and overcoated (right), reprinted with permission from ref. (88). Copyright 2011 American Chemical Society. b) HAADF-STEM image and corresponding EDX elemental maps for Al, O, Pb, Br, and Br+Al. c) EELS color-coded elemental intensity maps for Al and Br; b) and c) reprinted with permission from ref. (95). Copyright 2020 John Wiley and Sons.

3.3 Properties and applications

One of the major challenges when synthesizing ALD nanocomposites is to find the proper deposition conditions that do not compromise the NC properties. In the case of the QDs, the optical properties must be preserved especially when aiming at applications relying on light-matter interactions, such as solar cells and light emitting diodes. To study the effects of the ALD matrices on the QDs, optical features such as the excitonic peak position, the absorption peak width (full width at half-maximum (FWHM)) and photoluminescence emission peak have been monitored upon exposure of the samples to air, heat and light. Indeed, changes in these features correlate to changes of the QD size and size distribution. To give a specific example, in the

PbX/Al_2O_3 (X= S,Se) nanocomposites the excitonic peak position and its FWHM were used to quantify their stability against oxidation and sintering with and without the infilling matrix (**Figure 7a**).

As explained earlier, QDs, or more generally colloidal NCs, are constituted by a crystalline core surrounded by an organic ligand shell. This shell influences the optical and electronic properties by impacting the density of localized surface states via passivation of the under-coordinated surface atoms.[97]

In most of the studies reported above, the ALD deposition has resulted in a drop of the QD quantum yield (QY). A rare exception was reported by Jeannin et al.; however, in this case, CdSe QDs were embedded in thick ZnSe nanowires so somehow protected during the process.[98] Some hints that the interactions between the ALD precursors and the surface of the NCs are important were given by Devloo-Casier et al..[99] Here, the authors showed that a pre-treatment with TMA of the CdSe@ZnS core@shell QDs surface was needed to initiate the growth of the ALD ZnO coating; nevertheless the interaction of TMA with the surface was still causing the reduction of the QD QY (**Figure 7b**).

More recently Kuhs et al. performed a systematic in-situ PL study to monitor the PL changes of CdSe@CdS@ZnS core@shell QDs when exposed to different ALD precursors and environments (**Figure 7c**).[100] Particularly, the authors assessed the influence of vacuum, different plasmas (O_2, H_2O, H_2, H_2S/Ar, and Ar), precursors (TMA, diethylzinc (DEZ), tetrakis(dimethylamido)titanium (TDMAT), and tetrakis(ethylmethylamido)hafnium (TEMAHf)), co-reactants (H_2O, H_2S, and O_3), and ALD processes (growth of Al_2O_3, TiO_2, HfO_2, and ZnS) on QD film. They observed a PL reduction by up to 90% upon plasma treatments. They found that TMA and DEZ reduced the PL QY by more than 70% while exposure to TDMAT and TEMAHf

lowered the PL by only 10 − 20% (see **Figure 7c**). Lastly, while counterintuitive, water was identified to be crucial for maintaining a high PL.

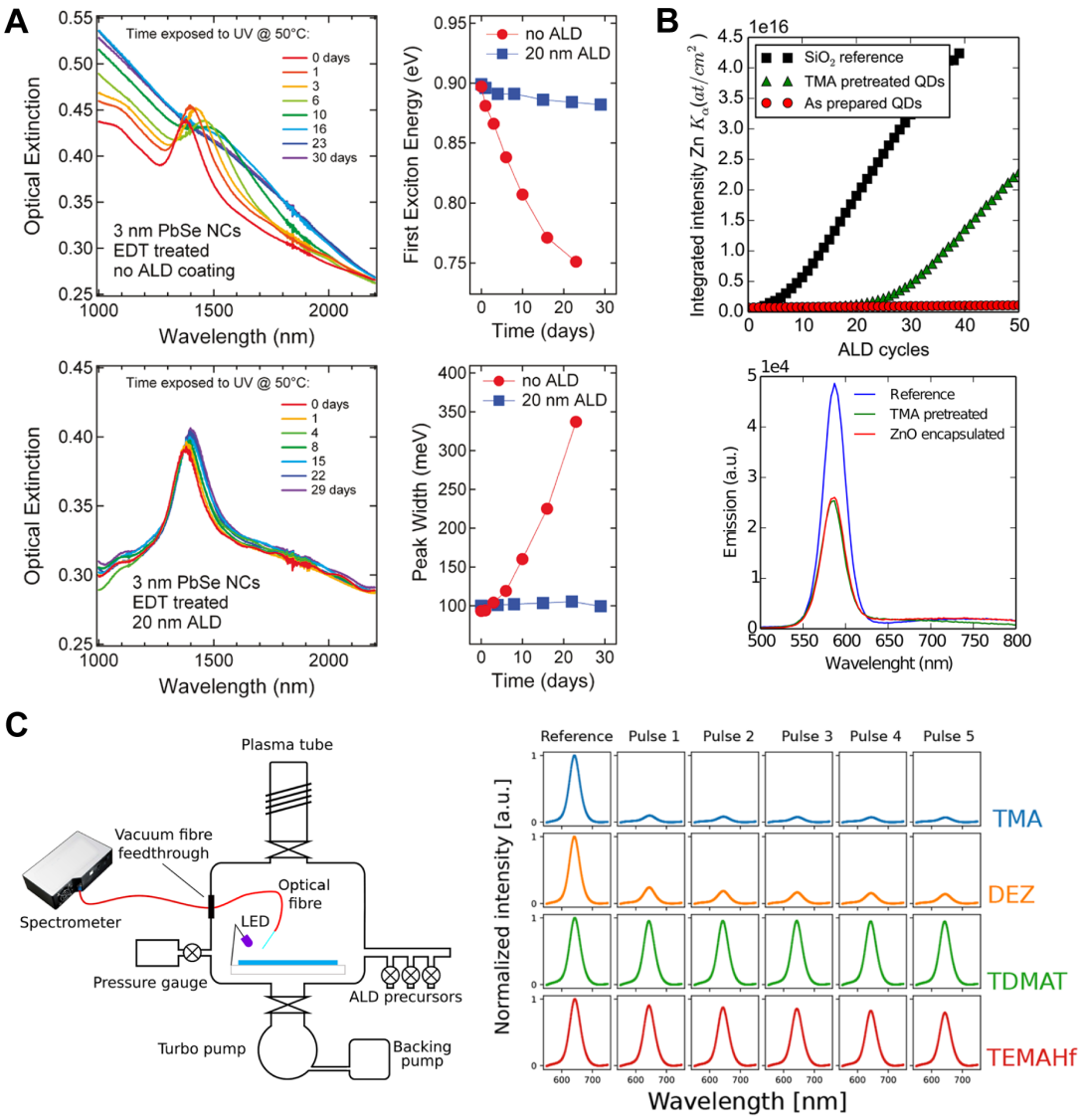

Figure 7. a) Optical absorption spectra of an uncoated (top) and infilled (bottom) EDT-treated film of 3 nm PbSe NCs exposed to UV light (365 nm, 1.4 mWcm^{-2}) at 50 ºC in a glovebox for 1 month together with the energy and width of the first exciton absorption peak over time for both samples, reprinted with permission from ref. (88). Copyright 2011 American Chemical Society. b) Integrated X-ray fluorescence (XRF) intensity of the Zn Kα line indicating the amount of deposited ZnO during the encapsulation process (top) and PL response for a monolayer of QDs before deposition after TMA pretreatment and after ZnO encapsulation (bottom), reprinted with permission from ref. (99). Copyright 2016 American Chemical Society. c) Schematic outline of the in situ ALD photoluminescence measurement setup (left) and normalized QD emission peak before and after 5x5 s exposure of TMA, DEZ, TDMAT and TEMAHf, reprinted with permission from ref. (100). Copyright 2019 American Chemical Society.

Nevertheless, in general, the reasons behind the PL reduction occurring during the ALD steps are not clear and some controversy still needs to be addressed. For example, Palei et al. have monitored the emission properties of CdSe@ZnS core@shell and CdSe@CdS dot-in-rods QDs during ALD alumina deposition.[93] Here, the authors observed that the PL intensity of the QD films was reduced with just a few ALD cycles, but then it recovered significantly once the infilling of the film was completed, which typically happens at 20−50 ALD cycles. Unfortunately, no reasoning of the phenomena was provided in this case. More recently, Bose et al. have explained the PL reduction by performing in-situ FTIR and ex-situ XPS for ALD alumina deposition on oleic acid-capped CdSe@CdS@ZnS QDs.[94] The interaction of the TMA with the surface of the QDs was found to induce a reorganization of ligand binding from Zn to Al and also significant loss of surface Zn atoms, both leading to PL intensity quenching.

Remaining in the general topic of optical properties for devices, carrier multiplication or also called multiple exciton generation is a phenomenon where the absorption of one photon of sufficiently high energy results in the generation of multiple electron−hole pairs of lower energy, highly beneficial for solar cells.[101] This phenomenon was observed in PbSe QDs dispersed in solution with high efficiency. Cate et al. demonstrated that the same occurs in 1,2-ethanedithiol-linked PbSe QD solids infilled with Al_2O_3 or Al_2O_3/ZnO with efficiency close to the one in solution, while it is negligible or absent in non-infilled films.[102]

In addition to the optical properties, transport properties of the nanocomposites also deserve attention, as they can be useful for all devices and especially for field effect transistors (FETs). As mentioned above, the ALD matrix combined with surface treatment (i.e. ligand removal or exchange with shorter ligands) can enhance carrier mobility within QD solids by lowering the height of the energetic barrier for inter-

quantum-dot transport.[89] So et al. have studied the effect of ALD on the electrical properties of alumina-passivated PbS QD films. Upon deposition, PbS QD film switch from p-type to ambipolar. In this case, the interstitial substitution of Pb sites by Al was found to be an important factor behind this change in properties, highlighting that diffusion-induced structural changes should also be taken into account during the ALD process. They also found that the infilling of pores with Al_2O_3 played an important role in enhancing of the air stability under ambient conditions.[103]

ALD coating for simple encapsulation has also produced a convenient, integrated packaging technology to increase the lifetime of QD solar cells and their performance. Ip et al. have shown that the encapsulation of a completed PbS QD solar cell with a 70-nm thick nanolaminate of Al_2O_3/ZnO deposited via ALD kept the same efficiency of 6% after being tested in air for a period of 13 days. The 70 nm nanolaminate overlayer was able to isolate the device from the atmospheric conditions without compromising the efficiency.[104] Lin et al. fabricated a QD and dye-sensitized solar cell with ALD TiO_2 as a barrier recombination layer. They reported a 41.3% improvement in the performance respect to the one without the ALD layer.[105] Roelofs et al. systematically studied the role of ALD Al_2O_3 films as blocking layers on solid state QD solar cells. Similar to previous reports, they observed that only 1 cycle of Al_2O_3 gave the highest efficiency in any configurations. The electron lifetime increased with the increase of Al_2O_3 thickness which support the conclusion that Al_2O_3 acts as a recombination barrier for the injected electrons into the TiO_2.[106]

Another advantage of the ALD overcoating is that its thickness can be precisely tuned and this is advantageous to study the electronic interactions between NC multilayers.[102,107–109] As one example, recently Saris et al. explored the capacity of

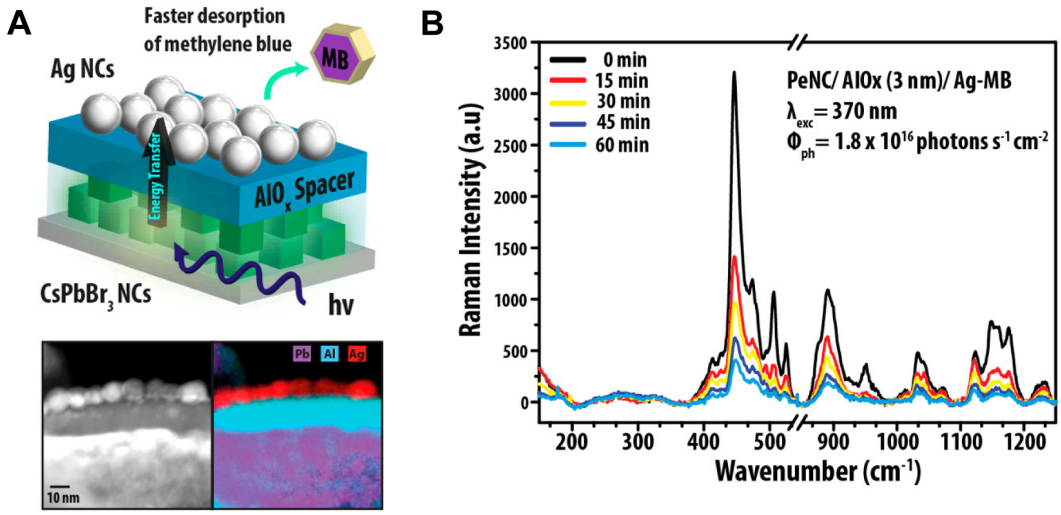

Figure 8. a) Schematic representation of the proposed $CsPbBr_3/AlO_x$/Ag NC antenna together with the cross-sectional HAADF-STEM image of the realized antenna and the corresponding EDX map. b) Representative photochemical reaction experiment showing the decrease of the Raman signal for the $CsPbBr_3/AlO_x$ (3 nm)/Ag-MB sample under illumination, all reprinted with permission from ref. (107). Copyright 2019 American Chemical Society.

$CsPbBr_3/AlO_x$ nanocomposite films to drive chemical reactions by coupling them to plasmonic Ag NCs. AlO_x was used both as a stabilizing layer and as a spacer to study distance-dependent excitation energy transfer, which revealed a migration of energy from the $CsPbBr_3$ QDs toward the Ag NCs (see **Figure 8**). This pooled energy was then utilized for a test reaction, specifically the methylene blue desorption. The results pointed at an improved efficiency with the nanocomposties compared to the single component system, most likely due to the extended spectral range absorption.

Finally, one interesting application of the nanocomposite including colloidal NCs coated with an ALD layer is to build functional hybrid materials by subsequent chemical transformations of the latter. For example, metal organic frameworks (MOFs) have been obtained by reacting the ALD oxide matrix with organic ligands. By this approach, NC/MOF nanocomposites comprising Ag NCs that are in intimate contact with Al-PMOF ([Al2(OH)$^{2-}$ (TCPP)]) (tetrakis(4-carboxyphenyl)porphyrin (TCPP)) matrix have been synthesized (**Figure 9a-c**).[110,111] Guntern et al. have demonstrated

that the synthesized NC/MOF nanocomposite can function as catalyst for the electrochemical CO_2 reduction reaction and tune the selectivity while conferring stability against sintering to the Ag NCs during operation. Moreover, they have also demonstrated that the same approach can be extended to other NCs such as gold and copper NCs of different size and shape.[83]

The concept of using the ALD coating as a precursor can be exploited further to synthesize different type of nanostructures. For example, Fan et al. have synthesized ZnO/Al_2O_3 core@shell nanowires (NWs) by coating ZnO NWs with 10 nm ALD Al_2O_3. Then, they transformed them into highly crystalline single phase spinel $ZnAl_2O_4$ nanotubes via an interfacial solid-state reaction and diffusion (**Figure 9d**).[112]

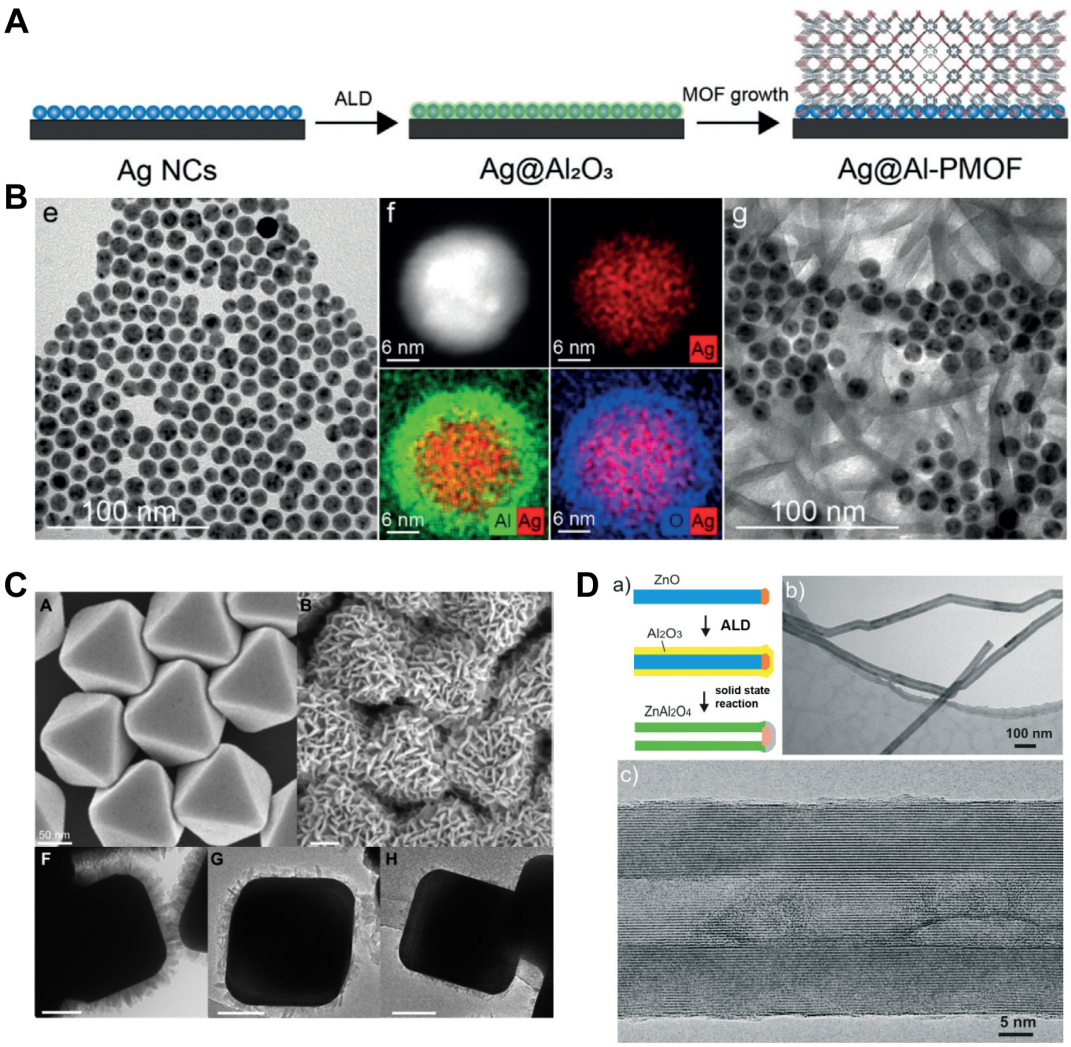

Figure 9. a) Scheme illustrating the synthesis of Ag/Al-PMOF hybrids. b) TEM and HAADF-STEM images with the corresponding EDX elemental maps for the Ag/Al_2O_3 core–shell particles after 45 ALD cycles and low-magnification TEM image of Ag/Al-PMOF hybrids; a) and b) reprinted with permission from ref. (110). Copyright 2019 John Wiley and Sons. c) Scanning electron microscopy (SEM) images of octahedral Ag NCs and AgNCs/MOF (top) and TEM images of Ag NC/MOF with different thickness obtained by tuning the number of ALD cycles. Scale bars = 50 nm. Reprinted with permission from ref. (111). Copyright 2015 American Chemical Society. d) Schematic diagram of the formation process of $ZnAl_2O_4$ spinel nanotubes together with TEM images of the obtained nanotubes, reprinted with permission from ref. (112). Copyright 2006 Nature Publishing Group.

4. Nanocrystalline heterostructures by coating colloidal NCs with a shell by c-ALD

4.1 State-of-the-art for the synthesis

A huge portfolio of NC heterostructures with different compositions and structures exists in the literature and their applications span from biomedical imaging to optical devices (such as LED and laser), solar energy harvesting devices and catalysis.[113-127] In this section, we focus on core@shell heterostructures where the core is constituted by NCs and the shell is grown by c-ALD.

As mentioned above, Ithurria et al. introduced a biphasic c-ALD process, which they used to deposit a CdS shell around CdSe QDs.[82] In a typical synthesis, the CdSe QDs are dispersed in the non-polar phase (i.e. toluene, hexane) while the K_2S for the growth of the shell is in the polar phase (i.e. dimethylformamide (FA)). The reaction occurs simply by vigorous agitation which induce temporarily mixing of the two solution. The nucleophilic S^{2-} ions react with the electron deficient Cd^{2+} sites at the NC surface and strip the native organic ligands, thus transferring the NCs to the polar phase. After this half cycle the upper phase is discarded and substituted with a fresh toluene solution

containing dodecyldimethylammonium bromide (DDAB) which transfers the NC back to the apolar phase. The addition of cadmium acetate to the fresh FA phase results in the growth of the Cd^{2+} layer, thus concluding the ALD cycle. The entire process must occur at room temperature as it is difficult to control the phase transfer otherwise. The synthesis scheme is reported in **Figure 10a.** The authors observed that the crystalline phase of the core (zinc-blende or wurtzite), the chemical composition of the cadmium and sulfide precursors and the nature of the phase-transfer agent were important parameter to obtain uniform isotropic or anisotropic shells around the CdSe cores. This discovery opened up a new pathway for the synthesis of heterostructured NCs motivating many researchers to apply the same to other compositions.

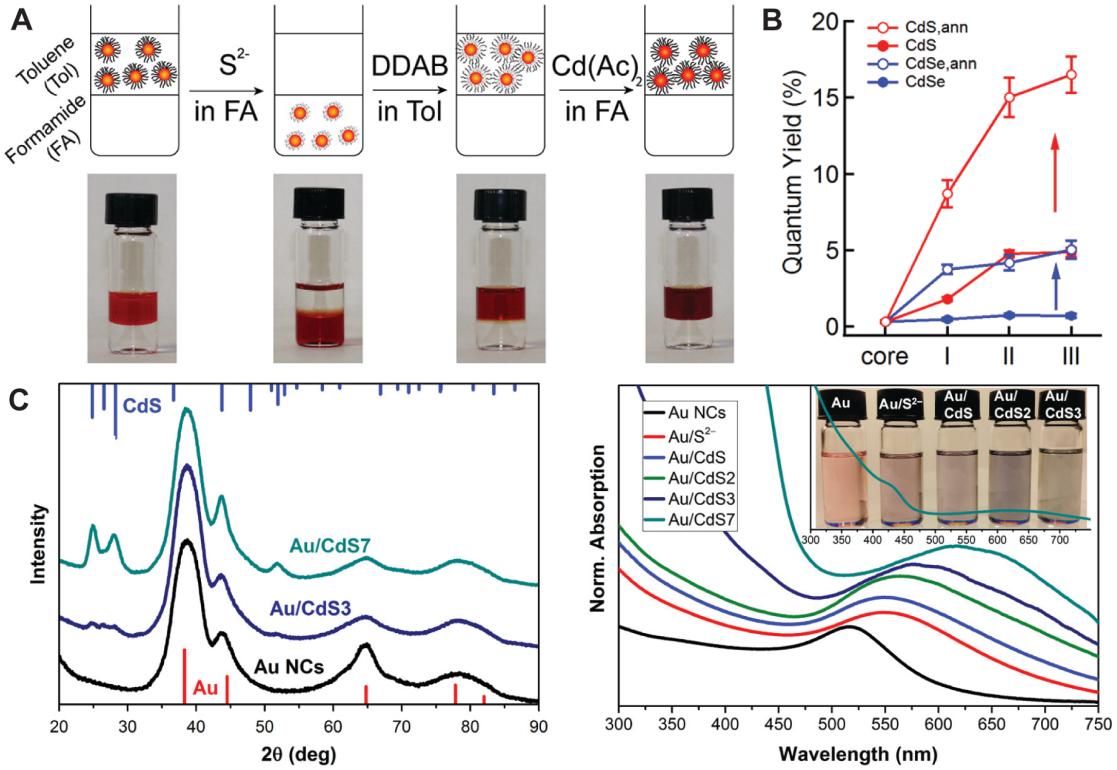

Figure 10. a) Schematics and photographs illustrating the c-ALD process for CdSe@CdS core@shell QDs, reprinted with permission from ref. (82). Copyright 2012 American Chemical Society. b) Comparison of absolute photoluminescence QY of HgSe@CdSe and HgSe@CdS core@shell QDs (full markers) before and (open markers) after annealing at 60 ºC in solution under an inert atmosphere, reprinted with permission from ref. (131). Copyright 2017 American Chemical Society. c) XRD patterns of the Au core, Au@3CdS, and Au@7CdS core@shell NCs (right) and

absorption spectra of the initial Au core (with diameter of ~4 nm) and core@shell Au@CdS NCs with varied shell thickness dissolved in toluene (left), reprinted with permission from ref. (132). Copyright 2017 American Chemical Society

For example, Sagar et al. proposed the room-temperature c-ALD to synthesize PbS@CdS core@shell heterostructures.[128] Before then, the most used method to obtain PbE@CdE (E=S, Se, Te) QDs was the so-called cation-exchange reaction, where the CdE shell is grown inward through the progressive exchange of Pb with Cd. However, the control of the interface composition and of the shell thickness was hardly possible through this approach. The c-ALD offered a much better alternative taking advantage that at room temperature the cation exchange of Pb with Cd is hindered, so a sharper interface, beneficial for the optoelectronic properties, can be obtained. Based on their absorption and Rutherford backscattering spectroscopy (RBS) measurements, the authors suggested that during the first half-cycle of the biphasic ALD process the S^{2-} ions react with the excess surface Pb^{2+} to form stoichiometric PbS QDs, while the subsequent cycles contribute to the CdS shell formation. Shortly after, Nasilowski et al.[129] also reported the synthesis of the same material by c-ALD with focus on the enhancement of the optical properties. Similarly to Sagar et al., the quantum yield (QY) of the obtained PbS@CdS heterostructures did not show the increment expected based on the results on PbS@CdS prepared by cation exchange.[130] However, the authors demonstrated that it could be recovered via addition of cadmium oleate after the c-ALD process, which suggests that defects were present on the surface.

Following their work on Pb-chalcogenide core@shell heterostructures, Sagar et al. conducted a similar study on Hg-chalcogenide QDs to synthesize HgSe@CdSe and Hg@CdSe heterostructures.[131] Due to their lower degeneracy of the band-edge states and shorter radiative lifetime, these materials are appealing for infrared optoelectronics. Enhanced QYs were obtained when the deposition was performed in inert conditions,

and even higher values were achieved when the samples are annealed at 60ºC for 45 minutes (**Figure 10b**). Moreover, through UV-vis absorption it was found that shell growth removes the n-doping, which is intrinsic to the native HgSe QD cores, thus becoming an interesting way to tune the intrinsic properties of these QDs.

Slejko et al. used c-ALD to create a big library of core@multishell structures which they used to tune the NC optoelectronic properties by means of wave function engineering.[132] For example, they grew alternating shells of ZnS and CdS around CdSe cores. By comparing CdSe@CdS, CdSe@CdS@ZnS@CdS@ZnS and CdSe @ZnS@CdS@ZnS with different number of layers per each shells, the authors identified the importance of the ZnS content in the heterostructures as well as of the interfaces to control electron delocalization in this system.

In a rather unique example, Razgoniaeva et al. used the biphasic c-ALD approach as a means to increase the NC size while maintaining the reaction in a size focusing regime which improves the final monodispersity of the sample. As a proof of concept, they grew shells of CdS around CdS seeds.[134]

Recently, Hazarika et al. have developed the biphasic c-ALD strategy further by eliminating the phase transfer step, that is difficult to control at elevated temperatures, in order to expanding the temperature range for the half-reactions. They selected reactants with low solubility in nonpolar reaction solvents, for example Li_2S, Li_2Se, $Cd(HCOO)_2$ and $Zn(OAc)_2$ in 1-octadecene. The reaction of a colloidal NC solution, in this case CdSe QDs and NPLs, with one of these solid reagents induces the half-reaction of the dissolved species with the NC surface and simultaneously shifts the equilibrium toward the dissolution of the solid reagents. After each half- cycle, the reagent salts are eliminated via decantation by centrifugation and co-solvent precipitation. This methodology allows performing the reaction at temperatures as high as150 ºC, thus

closer to the optimal conditions for nanomaterial synthesis.[128,131] With this new methodology the authors were able to synthesize an unprecedent library of II-VI semiconducting nanoplatelets heterostructures, as complex as 4CdSe@1CdS@3ZnCdS@1CdS@4CdSe@1CdS@3ZnCdS@1CdS@4CdSe (note: the numbers indicate the number of layers), with control down to one atomic layer.

From the discussion above, it is clear that most of the work on c-ALD has focused on chalcogenides. In an isolated example, Slejko et al. did prove that the methodology is also suitable to integrate components with intrinsically different characteristics in one nanoscale unit by synthesizing Au@CdS core@shell NCs, even though the lattice mismatch between these materials is significant. Usefully, X-ray diffraction (XRD) allowed the characterization of Au@CdS, showing the reflections of Au fcc and CdS wurtzite phases, the latter with increasing intensities as the shell thickness increases (**Figure 10c**). These heterostructures were also characterized by absorption spectroscopy; the enhanced plasmon-exciton interaction can explain the spectra broadening while the increase of the effective dielectric constant around the plasmonic Au NCs causes the red-shifting of the localized surface plasmon resonance (**Figure 10c**).

Only very recently, efforts towards applying the c-ALD to the growth of metal oxide shells have emerged. This late start might be related to multiple factors, including the lower reactivity of the precursors typically used for metal oxides (i.e. metal alkoxides) and the need of water as the co-reactants, which is not compatible with sensitive cores like QDs. Loiudice et al. have introduced a c-ALD approach to growth a tunable alumina shell around a variety of NC cores, including $CsPbX_3$ (where X = Cl, Br, I), CeO_2 and Ag. Here, the NCs are dispersed in an octane solution in a reaction flask where TMA and O_2 are sequentially introduced at room temperature (Figure 3b). The

purging of excess O_2 occurs by flowing N_2 for 5min between one half cycle and the following. The applicability of the synthesis to sensitive cores, like $CsPbX_3$ NCs, was possible thanks to the use of O_2 rather, instead of water, as the co-reactant.[84] In the process, the NC colloidal stability was preserved by regular additions of a stabilizing ligand (hrein oleic acid) that functionalizes the surface of the shell, allowing its further growth without any precipitation (see **Figure 11a**).

In a slightly different approach, Le Monnier et al. have used stoichiometrically limited injections to grow alumina and aluminum phosphate shells on dispersed powders of high surface area SiO_2 spheres (**Figure 11b**).[83] The reaction of the aluminum precursor (again TMA) with the SiO_2 spheres is possible thanks to the presence of hydroxyl groups on the spheres surface; the release of methane when TMA reacts with those hydroxyl groups permits to titrate the surface with the precursors, and then titrate a precursor-saturated surface with the co-reactant, assuring that the reaction is performed in stoichiometric conditions. Here, water is used as the co-reactant and therefore the method might not be applicable to cores sensitive to moisture such as QDs.

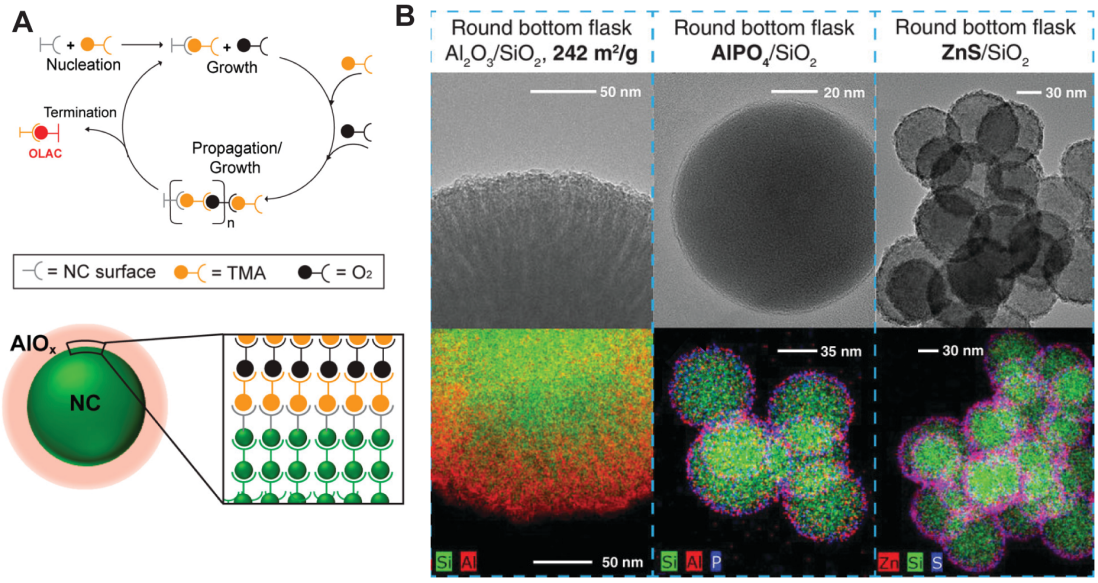

Figure 11. a) Schematic of the c-ALD synthesis to grow alumina shells on NCs of different nature, reprinted with permission from ref. (84). Copyright 2019 American Chemical Society. b) Bright-field TEM images of high-surface-area silica nanoparticles

coated with 10 cycles of TMA/ H_2O, $AlPO_4$ deposited onto silica particles replacing H_2O by H_3PO_4 as a counter-reactant and ZnS deposited onto silica spheres by the same liquid phase method using diethyl zinc and hydrogen sulfide as reactants (top row, left to right). Elemental mapping of the corresponding coated samples above using STEM with an EDX detector (bottom row). Reprinted with permission from ref. (83). Copyright 2019 John Wiley and Sons.

4.2 Characterization techniques

As discussed for the nanocomposites, because of their sensitivity to size and surface, optical properties have been extensively used to monitor the c-ALD processes on QDs. Indeed, many examples have been already given in the previous paragraph.[76,82,132,133,135] For the deposition processes that cannot be monitored with optical spectroscopies, such as the growth of metal oxide shells, dynamic light scattering (DLS) can be regarded as an alternative techniques. For example, DLS has been successfully used to follow the deposition and growth rate of alumina shells on $CsPbBr_3$ QDs (**Figure 12a).**[84]

Electron microscopy is certainly the most used and reliable tools to characterize the NC heterostructures obtained by c-ALD. In this case, the sample preparation is straightforward as it consists only in the deposition of a solution drop on a grid. In particular, high resolution TEM (HR-TEM) allows to gain insights into the interface between the core and the shell, which is important to better understand the arising properties. For example Hazarika et al. used HR-TEM coupled with electronic structure calculations to link quantum confinement and strain affect to the optical properties of the semiconductor nanostructures.[133] High resolution HAADF-STEM is another widely used technique to characterize core@shell structures (**Figure 12b**). This technique is sensitive to the atomic number of the elements (lighter elements result in brighter images), thereby enabling differentiation between core and shell. When coupled with spectroscopic techniques such as EDXS, HAADF-STEM becomes extremely helpful especially when the shell is amorphous (**Figure 12c**).[131]

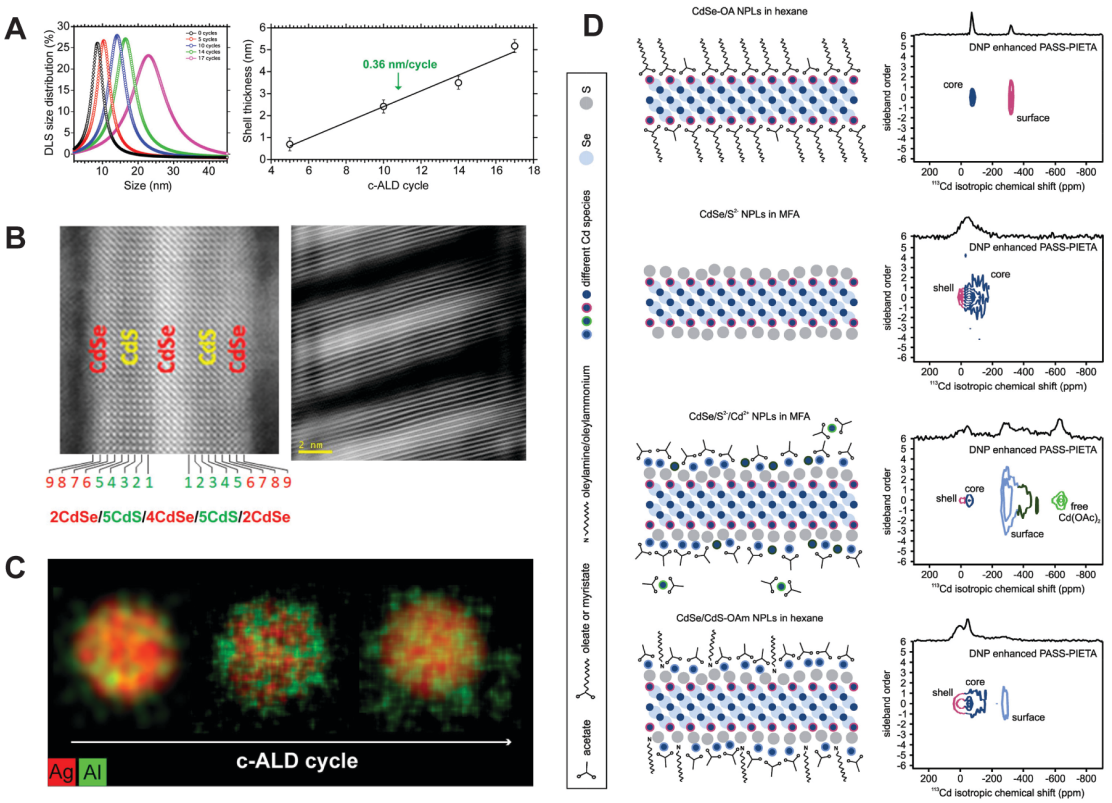

Figure 12. a) DLS size distribution of CsPbBr3@AlO_x NCs obtained by performing 0, 5, 10, 14, and 17 c-ALD cycles (left). Calculated shell thickness estimated by DLS measurements as a function of c-ALD cycles fitted with a linear curve (right). A growth rate of 0.36 nm/cycle is estimated which approximately corresponds to the Al-O bond length. Reprinted with permission from ref. (84). Copyright 2019 American Chemical Society. b) High-resolution HAADF-STEM image of 4CdSe/ 5CdS/4CdSe/5CdS/4CdSe NPL heterostructure (left) and HAADF-STEM image of 2CdS/2ZnS/2CdS/4CdSe/2CdS/2ZnS/2CdS NPL heterostructures (right). Reprinted with permission from ref. (133). Copyright 2019 American Chemical Society. c) EDX maps of Ag@AlO_x NCs obtained at different c-ALD cycles. Reprinted with permission from ref. (84). Copyright 2019 American Chemical Society. d) Schemes of the different steps of the c-ALD growth of one CdS monolayer onto CdSe NPLs, along with the corresponding DNP enhanced PASS-PIETA spectra. The color coding of the Cd atoms in the schemes indicates to which signal they belong to in the corresponding DNP enhanced PASS-PIETA spectrum. Reprinted with permission from ref. (136). Copyright 2020 American Chemical Society.

XRD is another standard tool to characterize NC heterostructures. Indeed strain arising from the shelling might cause lattice contraction or expansion which will result in changes in the peak position or width in the diffractograms.[128,131,132]

Despite NMR has been long used to study ligands on NCs,[136–138] only recently Piveteau et al. proposed solid state NMR to study the c-ALD step-wise growth of CdS shells on

CdSe NPLs.[139] Because of the low abundant active nuclei on surface, dynamic nuclear polarization (DNP) enhanced phase adjusted spinning sidebands-phase incremented echo-train acquisition (PASS-PIETA) was used. With this technique, they were able to successfully assign the NMR signals to core, shell and surface species, as well as in solution, thereby confirming the hypothesized mechanism of the biphasic c-ALD procedure (**Figure 12d**).

4.3 Properties and applications

Many examples of the optical properties of core@shell QDs obtained by c-ALD have been already discussed above. However, because of their intriguing behavior, the heterostructures including NPLs deserve some additional attention.[135] These NPLs are two-dimensional materials with non-confined lateral dimensions but with a small number of monolayers in the thickness, which therefore represents the dimension of quantum confinement.[140,141]

Because NPLs have been considered as the colloidal equivalent of quantum wells (QWs), She et al. considered the possibility to use them as media for laser gain (amplified spontaneous emission (ASE)).[142] They studied CdSe NPLs and xCdS@CdSe@xCdS ($x \leq 8$) and results showed that films of NPLs are superior medium for light amplification and optical gain than their QDs counterparts: 4-fold increased gain than the highest QDs reported and two orders of magnitude higher gain saturation value regarding the threshold value, comparing the 2-fold for QDs. The poorer performance of the QDs was attributed to the rapid nonradiative Auger recombination. As seen in **Figure 13a**, shell@core@shell NPLs show improved performances than CdSe NPLs only, but no clear dependence of the results with shell thickness was disclosed; the authors performed a full study with 3CdS@CdSe@3CdS

heterostructure, as it was the one which showed the lowest threshold value (8.6 μJ cm^{-2}).

In addition to their optical properties, the transport properties of NPLs are also impacted by the shell growth. To cite one example, Lhuillier et al. integrated CdSe@CdSe core@shell heterostructures synthesized by c-ALD in electrolyte-gated FET.[143] They found that the threshold voltage increases and saturates after the addition of the CdSe shell, which is indicative of induced stoichiometry defects during the c-ALD. Finally, they demonstrated how the film charging properties are affected by the organization of the nanoparticles. CdSe core only NPLs tend to stack, and these very dense films are poorly permeable to the diffusion of the electrolyte cations, thus films cannot be properly charged. The roughness induced by the CdSe shell (observed by TEM as well) allows a successful n-type charging of the films.

As for the very recently introduced c-ALD metal oxide shells, only a few applications have been reported so far.

In the work by Loiudice et al., the tunable metal oxide shell around $CsPbBr_3$ QDs was used to perform careful distance-dependence studies on the transfer of excitonic energy in semiconductor QDs films.[144] In a binary system composed by $CsPbBr_3$@AlO_x (donor) and CdSe NPLs (acceptor), results showed that the electronic interactions between the CsPbBr3 NCs and the CdSe nanoplatelets can be tuned from electron to energy transfer by increasing the shell thickness, thus enabling to target the desired system depending on the final application (**Figure 13b**). For example, the finding that energy transfer can take place for this highly emissive donors unlocks the opportunity for new operation motifs for devices such as lasers and light-emitting diodes. The same oxide shell enabled also in-situ XRD investigation of anion exchange reaction among $CsPbX_3$ (where X = Cl, Br, I) NCs. Those kind of studies were impeded before by the

fast exchange kinetics of the nanoscale exchange reaction, that were slowdown thanks to the presence of the metal oxide shell.[84]

Le Monnier et al. proved that the liquid-phase ALD grown metal oxide shells are useful for catalyst protection against sintering deactivation. Specifically, while coated palladium nanoparticles supported on silica showed less accessibility than uncoated ones, they remained unaffected by thermal treatments, while the dispersion of the uncoated Pd NPs on the support decreased as a result of sintering (**Figure 13c**).[83]

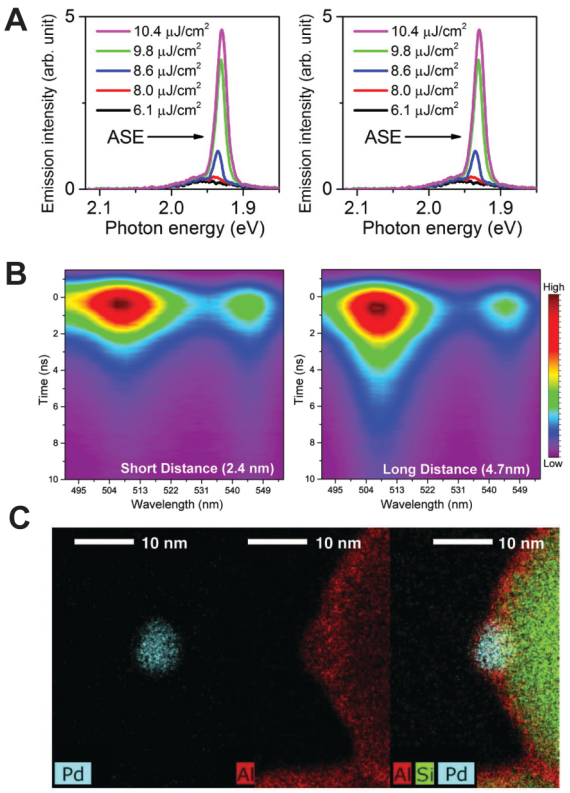

Figure 13. a) Emission spectra from films of CdSe (left) and 3CdS/CdSe/3CdS NPLs (right) for different pump fluences, reprinted with permission from ref. (142). Copyright 2014 American Chemical Society. b) Time- and energy-resolved PL intensity maps for short distance (2.4 nm) and long distance (4.7 nm) in equimolar binary mixtures of $CsPbBr_3$@AlO_x (donor) and CdSe NPLs (acceptor), reprinted with permission from ref. (144). Copyright 2019 American Chemical Society. c) STEM-EDX pictures of supported palladium nanoparticles on silica coated with 20 cycles of stoichiometrically injected alumina, reprinted with permission from ref. (83). Copyright 2019 John Wiley and Sons.

5. Conclusions and outlook

In this contribution, we have presented the wide range of nanocomposites and heterostructures attainable when colloidal chemistry is combined with gas-phase ALD and with the colloidal analogous, c-ALD, which has more recently been developed. We have highlighted the advancements made for the synthesis and how the properties are affected in these atomically-controlled multicomponent nanomaterials along with presenting some of the possible applications. Nevertheless, much room remains to further develop some of the concepts presented herein, and to bring new ideas to the field. Here, we conclude with our perspective on two of the open challenges which we believe will unlock new opportunities while being addressed.

5.1 Challenges of gas-phase ALD on nanostructured substrates

As discussed above, gas-phase ALD has the unique capability to grow uniform and conformal coatings on 3D structures with complex shapes, large aspect ratios and porous as opposed to other deposition techniques such as CVD, PVD and sol-gel.[50–52] Nevertheless, when the features of the substrate go down to the nanometer scale, some specific issues arise.[145] Furthermore, very few fundamental and modelling studies have focused on ALD coatings for materials with sub-30 nm pores, which is the case for NC films.[146,147]

To mention one of the challenges, the pores in a NC films could be easily clogged at the beginning of the deposition, making it difficult for reactant molecules to diffuse deeper into the structure. One solution to clogging is to use the ALD in the so-called exposure mode. At a given chamber pressure, a minimum time is needed before the sample surface is fully covered with adsorbed reactant molecules and saturation is reached. The product of the reactant partial pressure and the pulse time provides a useful measure for the reactant exposure time. To have a better conformality and compensate

for diffusion limitation much larger exposures are commonly required during ALD on high aspect ratio structures. Saris et al. have recently showed indeed that the exposure mode is preferable over the conventional mode for the synthesis of $CsPbBr_3/AlO_x$ nanocomposite for improved gas barrier properties of the alumina matrix.[148] The authors attributed this result to a better diffusion of the ALD precursors throughout the QD film, which indeed guarantees a more uniform nucleation on the entire QD surface.[148]

A second challenge is the tendency to sinter of most NCs at elevated temperatures, which is aggravated by the possible ligand desorption possibly induced by the vacuum inside the ALD reactor chamber. Most of the thermal ALD processes operate at relatively high temperatures (80–300 °C) in order to guarantee sufficient thermal energy to the precursor to react. These conditions are often incompatible with the maximum temperature affordable by the NCs. Therefore, future development in ambient-pressure ALD are desirable. For example, recently Valdesueiro et al. have deposited alumina on PbSe QDs at room temperature and atmospheric pressure using a custom-made ALD reactor.[149] Another potential solution is to use the c-ALD to growth a thin barrier layer material,such as alumina, around the NCs, and then to use gas-phase ALD to growth the matrix at higher temperature. The shell grown by c-ALD should prevent the sintering of the NCs and improve the infilling.[84]

Finally, the choice of the precursor should be carefully pondered, especially when ALD is applied to sensitive NC cores. In addition to the decomposition temperature and to the diffusion properties through narrow pores of the precursor itself, the compatibility of eventual reaction byproducts should be considered. For example, HCl formed from chloride-containing precursors represents a big challenge for many NCs as it could degrade them or induce shape changes. Additional information on selection of the ALD

precursors as well as a thorough summary of developed precursors can be found for in literature.[150,151]

5.2. The role of surface ligands during ALD synthesis

As already mentioned, organic ligands are crucial for the control of the composition and of the morphology of colloidal NCs. Furthermore, they are also important in determining the properties, as they bind to the NC surface, and in assuring the dispersibility of the NCs in a variety of solvents. Nevertheless, their role and fate during the nucleation and growth of the ALD coatings have not been extensively investigated so far.

One doubt that often arises for ALD nanocomposite is if the ligands are still bonded on the NC surface after the ALD process. On one side, ligand desorption might infer porosity to the ALD coating, a property which can be desirable for some applications (i.e. catalysis) but not when aiming at a barrier coating. On the other side, if ligands are still present on the surface, then their role during the ALD process must be assessed. FTIR and XPS depth profile analysis are useful techniques to answer this question. In the literature multiple studies agree that ligands are still present after the ALD process.[86,91,149] Valdesueiro et al. indicate that the ligands do indeed remain embedded in amine-capped PbSe QD/alumina nanocomposites; furthermore, the authors suggested that both the -OH groups on the QD surface and the amino-group in the ligands can react with the TMA during the first ALD steps.[149] In their study on ALD alumina deposition on CdTe QDs capped with short chain thiocarboxylic acid, Yin et al. suggest that the carboxylic termination is necessary to initiate the ALD nucleation which involve the reaction of the TMA with hydroxyl groups.[91] In their work on $CsPbBr_3$/alumina nanocomposite, Loiudice et al provide additional insights by proposing that the TMA reacts with the partially oxidized QD surface during the initial

stage of nucleation.[86] Upon saturation of the oxidized surface sites, the TMA molecules intercalate at the ligand/QD interface as proposed also by Li and co-workers.[152] This step introduces trap states and causes a decrease of QY, thus it should be prevented. Later on, the development of the c-ALD around NCs, allowed the authors to elucidate the mechanism further and to conclude that oxygen-sites, either on the NC surface or in the ligands stabilizing the NCs, are needed for nucleation.[84,95] Indeed, no shelling, but homogeneous nucleation, was observed when utilizing oleylamine-capped metal Ag NCs, while the AlO_x shell grew heterogeneously when the surface of the same NC was partially oxidized.[84] In general, more NMR studies should be performed in order to elucidate the entire process. While still rare, first efforts in this direction have proven to be extremely insightful.[139]

Ligand exchange procedures could also be used to optimize the c-ALD process. As one isolated example, Razgoniaeva et al. have showed that substituting the native oleic acid on CdSe with Na2S and oleylamine as the first step of the shelling process facilitates the adsorption of the S^{2-} co-reactant.[134] However, more strategies and for different systems could be developed building on the huge literature available on NC surface modifications.

Overall, elucidating the role of the ligands during the c-ALD process will both enable a more rational synthetic design and also shed light on some of the contrasting results reported for the same systems (i.e. different trends in the optical properties of CdSe@CdS prepared by c-ALD are reported in the literature[82,132]) or not fully explained changes of optical properties discussed above for the nanocomposites.

In the near future, strategies to confer functionality to the organic ligands by properly engineering the anchoring groups, so to serve as a nucleation point during the ALD

process, might be considered. This development can open future opportunities in selective area ALD by positioning such ligands only on specific facets of the NC cores.

References

(1) Singh, S.; Chen, H.; Shahrokhi, S.; Wang, L. P.; Lin, C.-H.; Hu, L.; Guan, X.; Tricoli, A.; Xu, Z. J.; Wu, T. Hybrid Organic–Inorganic Materials and Composites for Photoelectrochemical Water Splitting. *ACS Energy Lett.* **2020**, 1487–1497.

(2) Huang, Z.; Gong, J.; Nie, Z. Symmetry-Breaking Synthesis of Multicomponent Nanoparticles. *Acc. Chem. Res.* **2019**, *52* (4), 1125–1133.

(3) Bashir, S.; Liu, J. Overviews of Synthesis of Nanomaterials. In *Advanced Nanomaterials and Their Applications in Renewable Energy*; Liu, J. L., Bashir, S. B. T., Eds.; Elsevier, 2015; pp 51–115.

(4) Soon, G. K.; Hyeon, T. Colloidal Chemical Synthesis and Formation Kinetics of Uniformly Sized Nanocrystals of Metals, Oxides, and Chalcogenides. *Acc. Chem. Res.* **2008**, *41* (12), 1696–1709.

(5) Sasidharan, S.; Raj, S.; Sonawane, S.; Sonawane, S.; Pinjari, D.; Pandit, A. B.; Saudagar, P. Chapter 2 - Synthesis: Chemical and Biological Route and Applications. In *Nanomaterials Synthesis*; Beeran Pottathara, Y., Thomas, S., Kalarikkal, N., Grohens, Y., Kokol, V. B. T., Eds.; Elsevier, 2019; pp 27–51.

(6) Oviroh, P. O.; Akbarzadeh, R.; Pan, D.; Coetzee, R. A. M.; Jen, T.-C. New Development of Atomic Layer Deposition: Processes, Methods and Applications. *Sci. Technol. Adv. Mater.* **2019**, *20* (1), 465–496.

(7) Buonsanti, R.; Milliron, D. J. Chemistry of Doped Colloidal Nanocrystals. *Chem. Mater.* **2013**, *25* (8), 1305–1317.

(8) Cozzoli, P. D.; Pellegrino, T.; Manna, L. Synthesis, Properties and Perspectives of Hybrid Nanocrystal Structures. *Chem. Soc. Rev.* **2006**, *35* (11), 1195–1208.

(9) Shamsi, J.; Urban, A. S.; Imran, M.; De Trizio, L.; Manna, L. Metal Halide Perovskite Nanocrystals: Synthesis, Post-Synthesis Modifications, and Their Optical Properties. *Chem. Rev.* **2019**, *119* (5), 3296–3348.

(10) Nasilowski, M.; Mahler, B.; Lhuillier, E.; Ithurria, S.; Dubertret, B. Two-Dimensional Colloidal Nanocrystals. *Chem. Rev.* **2016**, *116* (18), 10934–10982.

(11) Yin, Y.; Alivisatos, A. P. Colloidal Nanocrystal Synthesis and the Organic-

Inorganic Interface. *Nature* **2005**, *437*, 664–670.

(12) Lee, S. M.; Cho, S. N.; Cheon, J. Anisotropic Shape Control of Colloidal Inorganic Nanocrystals. *Adv. Mater.* **2003**, *15* (5), 441–444.

(13) Yu, W. W.; Wang, Y. A.; Peng, X. Formation and Stability of Size-, Shape-, and Structure-Controlled CdTe Nanocrystals: Ligand Effects on Monomers and Nanocrystals. *Chem. Mater.* **2003**, *15* (22), 4300–4308.

(14) Sun, S.; Yuan, D.; Xu, Y.; Wang, A.; Deng, Z. Ligand-Mediated Synthesis of Shape-Controlled Cesium Lead Halide Perovskite Nanocrystals via Reprecipitation Process at Room Temperature. *ACS Nano* **2016**, *10* (3), 3648–3657.

(15) Strach, M.; Mantella, V.; Pankhurst, J. R.; Iyengar, P.; Loiudice, A.; Das, S.; Corminboeuf, C.; Van Beek, W.; Buonsanti, R. Insights into Reaction Intermediates to Predict Synthetic Pathways for Shape-Controlled Metal Nanocrystals. *J. Am. Chem. Soc.* **2019**, *141* (41), 16312–16322.

(16) Baranov, D.; Manna, L.; Kanaras, A. G. Chemically Induced Self-Assembly of Spherical and Anisotropic Inorganic Nanocrystals. *J. Mater. Chem.* **2011**, *21* (42), 16694–16703.

(17) Lee, H.; Yoon, D. E.; Koh, S.; Kang, M. S.; Lim, J.; Lee, D. C. Ligands as a Universal Molecular Toolkit in Synthesis and Assembly of Semiconductor Nanocrystals. *Chem. Sci.* **2020**, *11* (9), 2318–2329.

(18) Boles, M. A.; Engel, M.; Talapin, D. V. Self-Assembly of Colloidal Nanocrystals: From Intricate Structures to Functional Materials. *Chem. Rev.* **2016**, *116* (18), 11220–11289.

(19) Boles, M. A.; Talapin, D. V. Self-Assembly of Tetrahedral Cdse Nanocrystals: Effective “Patchiness” via Anisotropic Steric Interaction. *J. Am. Chem. Soc.* **2014**, *136* (16), 5868–5871.

(20) Buonsanti, R.; Grillo, V.; Carlino, E.; Giannini, C.; Kipp, T.; Cingolani, R.; Cozzoli, P. D. Nonhydrolytic Synthesis of High-Quality Anisotropically Shaped Brookite TiO2 Nanocrystals. *J. Am. Chem. Soc.* **2008**, *130* (33), 11223–11233.

(21) Loiudice, A.; Lobaccaro, P.; Kamali, E. A.; Thao, T.; Huang, B. H.; Ager, J. W.; Buonsanti, R. Tailoring Copper Nanocrystals towards C2 Products in Electrochemical CO2 Reduction. *Angew. Chemie - Int. Ed.* **2016**, *55* (19), 5789–5792.

(22) Kriegel, I.; Rodríguez-Fernández, J.; Wisnet, A.; Zhang, H.; Waurisch, C.; Eychmüller, A.; Dubavik, A.; Govorov, A. O.; Feldmann, J. Shedding Light on Vacancy-Doped Copper Chalcogenides: Shape-Controlled Synthesis, Optical Properties, and Modeling of Copper Telluride Nanocrystals with near-Infrared Plasmon Resonances. *ACS Nano* **2013**, *7* (5), 4367–4377.

(23) Iyengar, P.; Huang, J.; De Gregorio, G. L.; Gadiyar, C.; Buonsanti, R. Size Dependent Selectivity of Cu Nano-Octahedra Catalysts for the Electrochemical Reduction of CO2 to CH4. *Chem. Comm.* **2019**, *55* (60), 8796–8799.

(24) De Gregorio, G. L.; Burdyny, T.; Loiudice, A.; Iyengar, P.; Smith, W. A.; Buonsanti, R. Facet-Dependent Selectivity of Cu Catalysts in Electrochemical CO2 Reduction at Commercially Viable Current Densities. *ACS Catal.* **2020**, 4854–4862.

(25) Gadiyar, C.; Strach, M.; Schouwink, P.; Loiudice, A.; Buonsanti, R. Chemical Transformations at the Nanoscale: Nanocrystal-Seeded Synthesis of β-Cu2V2O7 with Enhanced Photoconversion Efficiencies. *Chem. Sci.* **2018**, *9* (25), 5658–5665.

(26) Huang, J.; Hörmann, N.; Oveisi, E.; Loiudice, A.; De Gregorio, G. L.; Andreussi, O.; Marzari, N.; Buonsanti, R. Potential-Induced Nanoclustering of Metallic Catalysts during Electrochemical CO2 Reduction. *Nat. Commun.* **2018**, *9* (1), 1–9.

(27) Reiss, P.; Carrière, M.; Lincheneau, C.; Vaure, L.; Tamang, S. Synthesis of Semiconductor Nanocrystals, Focusing on Nontoxic and Earth-Abundant Materials. *Chem. Rev.* **2016**, *116* (18), 10731–10819.

(28) Lee, J. M.; Kraynak, L. A.; Prieto, A. L. A Directed Route to Colloidal Nanoparticle Synthesis of the Copper Selenophosphate Cu3PSe4. *Angew. Chemie* **2020**, *132* (8), 3062–3066.

(29) Miller, R. C.; Neilson, J. R.; Prieto, A. L. Amide-Assisted Synthesis of Iron Germanium Sulfide (Fe2GeS4) Nanostars: The Effect of LiN(SiMe3)2 on Precursor Reactivity for Favoring Nanoparticle Nucleation or Growth. *J. Am. Chem. Soc.* **2020**, *142* (15), 7023–7035.

(30) Lu, X.; Korgel, B. A. A Single-Step Reaction for Silicon and Germanium Nanorods. *Chem. Eur. J.* **2014**, *20* (20), 5874–5879.

(31) Liu, W.; Chang, A. Y.; Schaller, R. D.; Talapin, D. V. Colloidal InSb Nanocrystals. *J. Am. Chem. Soc.* **2012**, *134* (50), 20258–20261.

(32) Steinhagen, C.; Panthani, M. G.; Akhavan, V.; Goodfellow, B.; Koo, B.; Korgel, B. A. Synthesis of Cu2ZnSnS4 Nanocrystals for Use in Low-Cost Photovoltaics. *J. Am. Chem. Soc.* **2009**, *131* (35), 12554–12555.

(33) Singh, A.; Geaney, H.; Laffir, F.; Ryan, K. M. Colloidal Synthesis of Wurtzite Cu2ZnSnS4 Nanorods and Their Perpendicular Assembly. *J. Am. Chem. Soc.* **2012**, *134* (6), 2910–2913.

(34) Gaspari, R.; Della Valle, G.; Ghosh, S.; Kriegel, I.; Scotognella, F.; Cavalli, A.; Manna, L. Quasi-Static Resonances in the Visible Spectrum from All-Dielectric Intermediate Band Semiconductor Nanocrystals. *Nano Lett.* **2017**, *17* (12), 7691–7695.

(35) Mantella, V.; Ninova, S.; Saris, S.; Loiudice, A.; Aschauer, U.; Buonsanti, R. Synthesis and Size-Dependent Optical Properties of Intermediate Band Gap Cu3VS4 Nanocrystals. *Chem. Mater.* **2019**, *31* (2), 532–540.

(36) Loiudice, A.; Ma, J.; Drisdell, W. S.; Mattox, T. M.; Cooper, J. K.; Thao, T.; Giannini, C.; Yano, J.; Wang, L. W.; Sharp, I. D.; Buonsanti, R. Bandgap Tunability in Sb-Alloyed BiVO4 Quaternary Oxides as Visible Light Absorbers for Solar Fuel Applications. *Adv. Mater.* **2015**, *27* (42), 6733–6740.

(37) Loiudice, A.; Cooper, J. K.; Hess, L. H.; Mattox, T. M.; Sharp, I. D.; Buonsanti, R. Assembly and Photocarrier Dynamics of Heterostructured Nanocomposite Photoanodes from Multicomponent Colloidal Nanocrystals. *Nano Lett.* **2015**, *15* (11), 7347–7354.

(38) Oh, M. H.; Yu, T.; Yu, S.-H.; Lim, B.; Ko, K.-T.; Willinger, M.-G.; Seo, D.-H.; Kim, B. H.; Cho, M. G.; Park, J.-H.; Kang, K.; Sung, Y.-E.; Pinna, N.; Hyeon, T. Galvanic Replacement Reactions in Metal Oxide Nanocrystals. *Science* **2013**, *340*, 964–969.

(39) Rivest, J. B.; Jain, P. K. Cation Exchange on the Nanoscale: An Emerging Technique for New Material Synthesis, Device Fabrication, and Chemical Sensing. *Chem. Soc. Rev.* **2013**, *42* (1), 89–96.

(40) Wang, W.; Dahl, M.; Yin, Y. Hollow Nanocrystals through the Nanoscale Kirkendall Effect. *Chem. Mater.* **2013**, *25* (8), 1179–1189.

(41) Fritzinger, B.; Moreels, I.; Lommens, P.; Koole, R.; Hens, Z.; Martins, J. C. In Situ Observation of Rapid Ligand Exchange in Colloidal Nanocrystal Suspensions Using Transfer NOE Nuclear Magnetic Resonance Spectroscopy. *J. Am. Chem. Soc.* **2009**, *131* (8), 3024–3032.

(42) Abolhasani, M.; Coley, C. W.; Xie, L.; Chen, O.; Bawendi, M. G.; Jensen, K. F. Oscillatory Microprocessor for Growth and in Situ Characterization of Semiconductor Nanocrystals. *Chem. Mater.* **2015**, *27* (17), 6131–6138.

(43) Qu, L.; Yu, W. W.; Peng, X. In Situ Observation of the Nucleation and Growth of CdSe Nanocrystals. *Nano Lett.* **2004**, *4* (3), 465–469.

(44) Mantella, V.; Strach, M.; Frank, K.; Pankhurst, J. R.; Stoian, D.; Gadyiar, C.; Nickel, B.; Buonsanti, R. Polymer Lamellae as Reaction Intermediates of Copper Nanospheres Evidenced by In-situ X-ray Studies. *Angew. Chemie - Int. Ed. Int. Ed.* **2020**, *59*, 2–9.

(45) Antson, J.; Suntola, T. U.S. Patent 4,058,430, 1977.

(46) Guan, C.; Wang, J. Recent Development of Advanced Electrode Materials by Atomic Layer Deposition for Electrochemical Energy Storage. *Adv. Sci.* **2016**, *3* (10), 1–23.

(47) Asundi, A. S.; Raiford, J. A.; Bent, S. F. Opportunities for Atomic Layer Deposition in Emerging Energy Technologies. *ACS Energy Lett.* **2019**, *4* (4), 908–925.

(48) Chatham, H. Oxygen Diffusion Barrier Properties of Transparent Oxide Coatings on Polymeric Substrates. *Surf. Coatings Technol.* **1996**, *78*, 1–9.

(49) Lim, J. S.; Kim, Y. K.; Choi, S. J.; Lee, J. H.; Kim, Y. S.; Lee, B. T.; Park, H. S.; Park, Y. W.; Lee, S. I. Novel Al2O3 Capacitor for High Density DRAMs. In *ICVC 1999 - 6th International Conference on VLSI and CAD*; 1999; pp 506–509.

(50) Choi, G.; Satyanarayana, L.; Park, J. Effect of Process Parameters on Surface Morphology and Characterization of PE-ALD SnO2 Thin Films for Gas Sensing. *Appl. Surf. Sci.* **2006**, *252* (22), 7878–7883.

(51) Ginley, D.; Coutts, T.; Perkins, J.; Young, D.; Li, X.; Parilla, P. Next-Generation Transparent Conducting Oxides for Photovoltaic Cells: An Overview. *MRS Proc.* **2001**, *668*, H2.7.

(52) Ritala, M.; Niinistö, J. Atomic Layer Deposition. In *Chemical Vapour Deposition: Precursors, Processes and Applicaions*; Jones, A. C., Hitchman, M. L., Eds.; Royal Society of Chemistry, 2009; pp 158–206.

(53) George, S. M. Atomic Layer Deposition: An Overview. *Chem. Rev.* **2010**, *110* (1), 111–131.

(54) McDonnell, S. J.; Wallace, R. M. UV-Ozone Functionalization of 2D

Materials. *JOM* **2019**, *71* (1), 224–237.

(55) Profijt, H. B.; Potts, S. E.; van de Sanden, M. C. M.; Kessels, W. M. M. Plasma-Assisted Atomic Layer Deposition: Basics, Opportunities, and Challenges. *J. Vac. Sci. Technol. A* **2011**, *29* (5), 050801.

(56) Nicolau, Y. F. Solution Deposition of Thin Solid Compound Films by a Successive Ionic-Layer Adsorption and Reaction Process. *Appl. Surf. Sci.* **1985**, *22–23* (PART 2), 1061–1074.

(57) Park, S.; Clark, B. L.; Keszler, D. A.; Bender, J. P.; Wager, J. F.; Reynolds, T. A.; Herman, G. S. Low-Temperature Thin-Film Deposition and Crystallization. *Science* **2002**, *297* (5578), 65.

(58) Sartale, S. D.; Lokhande, C. D. Studies on Large Area (∼50 Cm2) MoS2 Thin Films Deposited Using Successive Ionic Layer Adsorption and Reaction (SILAR) Method. *Mater. Chem. Phys.* **2001**, *71* (1), 94–97.

(59) Kanniainen, T.; Lindroos, S.; Ihanus, J.; Leskelä, M. Growth of Lead Selenide Thin Films by the Successive Ionic Layer Adsorption and Reaction (SILAR) Technique. *J. Mater. Chem.* **1996**, *6* (6), 983–986.

(60) Niinistö, L.; Kanniainen, T.; Lindroos, S.; Resch, R.; Leskelä, M.; Friedbacher, G.; Grasserbauer, M. Growth of Zinc Sulfide Thin Films on with the Successive Ionic Layer Adsorption and Reaction Method as Studied by Atomic Force Microscopy. *J. Mater. Chem.* **1995**, *5* (7), 985–989.

(61) Lindroos, S.; Leskelä, M. Growth of Zinc Peroxide (ZnO2) and Zinc Oxide (ZnO) Thin Films by the Successive Ionic Layer Adsorption and Reaction - SILAR - Technique. *Int. J. Inorg. Mater.* **2000**, *2* (2–3), 197–201.

(62) Su, Z.; Sun, K.; Han, Z.; Liu, F.; Lai, Y.; Li, J.; Liu, Y. Fabrication of Ternary Cu-Sn-S Sulfides by a Modified Successive Ionic Layer Adsorption and Reaction (SILAR) Method. *J. Mater. Chem.* **2012**, *22* (32), 16346–16352.

(63) Sun, K.; Su, Z.; Yan, C.; Liu, F.; Cui, H.; Jiang, L.; Shen, Y.; Hao, X.; Liu, Y. Flexible Cu2ZnSnS4 Solar Cells Based on Successive Ionic Layer Adsorption and Reaction Method. *RSC Adv.* **2014**, *4* (34), 17703–17708.

(64) Suryawanshi, M. P.; Ghorpade, U. V.; Suryawanshi, U. P.; He, M.; Kim, J.; Gang, M. G.; Patil, P. S.; Moholkar, A. V.; Yun, J. H.; Kim, J. H. Aqueous-Solution-Processed Cu2ZnSn(S,Se)4 Thin-Film Solar Cells via an Improved Successive Ion-Layer-Adsorption Reaction Sequence. *ACS Omega* **2017**, *2* (12), 9211–9220.

(65) Zhou, R.; Zhang, Q.; Tian, J.; Myers, D.; Yin, M.; Cao, G. Influence of Cationic Precursors on CdS Quantum-Dot-Sensitized Solar Cell Prepared by Successive Ionic Layer Adsorption and Reaction. *J. Phys. Chem. C* **2013**, *117* (51), 26948–26956.

(66) Abbas, M. A.; Basit, M. A.; Park, T. J.; Bang, J. H. Enhanced Performance of PbS-Sensitized Solar Cells via Controlled Successive Ionic-Layer Adsorption and Reaction. *Phys. Chem. Chem. Phys.* **2015**, *17* (15), 9752–9760.

(67) Lee, H.; Wang, M.; Chen, P.; Gamelin, D. R.; Zakeeruddin, S. M.; Grätzel, M.; Nazeeruddin, M. K. Efficient CdSe Quantum Dot-Sensitized Solar Cells Prepared by an Improved Successive Ionic Layer Adsorption and Reaction Process. *Nano Lett.* **2009**, *9* (12), 4221–4227.

(68) Shaikh, S. F.; Ghule, B. G.; Nakate, U. T.; Shinde, P. V.; Ekar, S. U.; O'Dwyer, C.; Kim, K. H.; Mane, R. S. Low-Temperature Ionic Layer Adsorption and Reaction Grown Anatase TiO2 Nanocrystalline Films for Efficient Perovskite Solar Cell and Gas Sensor Applications. *Sci. Rep.* **2018**, *8* (1), 1–11.

(69) Shei, S. C.; Zeng, X. F.; Lin, N. M.; Chang, S. J. SiNx Nanopillars on AlGaInP-Based Light-Emitting Diodes to Enhance Light Extraction Using Self-Assembly ZnO Nanomask Coating by Successive Ionic Layer Adsorption and Reaction Method. *Thin Solid Films* **2014**, *570* (PB), 230–234.

(70) Jana, M.; Saha, S.; Samanta, P.; Murmu, N. C.; Kim, N. H.; Kuila, T.; Lee, J. H. Growth of Ni-Co Binary Hydroxide on a Reduced Graphene Oxide Surface by a Successive Ionic Layer Adsorption and Reaction (SILAR) Method for High Performance Asymmetric Supercapacitor Electrodes. *J. Mater. Chem. A* **2016**, *4* (6), 2188–2197.

(71) Jana, M.; Saha, S.; Samanta, P.; Murmu, N. C.; Kim, N. H.; Kuila, T.; Lee, J. H. A Successive Ionic Layer Adsorption and Reaction (SILAR) Method to Fabricate a Layer-by-Layer (LbL) MnO2-Reduced Graphene Oxide Assembly for Supercapacitor Application. *J. Power Sources* **2017**, *340*, 380–392.

(72) Dubal, D. P.; Holze, R. A Successive Ionic Layer Adsorption and Reaction (SILAR) Method to Induce Mn3O4 Nanospots on CNTs for Supercapacitors. *New J. Chem.* **2013**, *37* (2), 403–408.

(73) Treml, B. E.; Savitzky, B. H.; Tirmzi, A. M.; Dasilva, J. C.; Kourkoutis, L. F.; Hanrath, T. Successive Ionic Layer Absorption and Reaction for Postassembly

Control over Inorganic Interdot Bonds in Long-Range Ordered Nanocrystal Films. *ACS Appl. Mater. Interfaces* **2017**, *9* (15), 13500–13507.

(74) Oh, S. J.; Berry, N. E.; Choi, J. H.; Gaulding, E. A.; Lin, H.; Paik, T.; Diroll, B. T.; Muramoto, S.; Murray, C. B.; Kagan, C. R. Designing High-Performance PbS and PbSe Nanocrystal Electronic Devices through Stepwise, Post-Synthesis, Colloidal Atomic Layer Deposition. *Nano Lett.* **2014**, *14* (3), 1559–1566.

(75) Li, J. J.; Wang, Y. A.; Guo, W.; Keay, J. C.; Mishima, T. D.; Johnson, M. B.; Peng, X. Large-Scale Synthesis of Nearly Monodisperse CdSe/CdS Core/Shell Nanocrystals Using Air-Stable Reagents via Successive Ion Layer Adsorption and Reaction. *J. Am. Chem. Soc.* **2003**, *125* (41), 12567–12575.

(76) Greytak, A. B.; Tan, R.; Roberts, S. K. Prospects for Rational Control of Nanocrystal Shape Through Successive Ionic Layer Adsorption and Reaction (SILAR) and Related Approaches. In *Anisotropic and Shape-Selective Nanomaterials*; Murph, S. E. H., Larsen, G. K., Coopersmith, K. J., Eds.; Springer, 2017; pp 169–232.

(77) Tan, R.; Blom, D. A.; Ma, S.; Greytak, A. B. Probing Surface Saturation Conditions in Alternating Layer Growth of CdSe/CdS Core/Shell Quantum Dots. *Chem. Mater.* **2013**, *25* (2), 3724–3736.

(78) Xie, R.; Kolb, U.; Li, J.; Basché, T.; Mews, A. Synthesis and Characterization of Highly Luminescent CdSe-Core CdS/Zn 0.5Cd0.5S/ZnS Multishell Nanocrystals. *J. Am. Chem. Soc.* **2005**, *127* (20), 7480–7488.

(79) Chen, Y.; Vela, J.; Htoon, H.; Casson, J. L.; Werder, D. J.; Bussian, D. A.; Klimov, V. I.; Hollingsworth, J. A. "Giant" Multishell CdSe Nanocrystal Quantum Dots with Suppressed Blinking. *J. Am. Chem. Soc.* **2008**, *130* (15), 5026–5027.

(80) Dennis, A. M.; Mangum, B. D.; Piryatinski, A.; Park, Y. S.; Hannah, D. C.; Casson, J. L.; Williams, D. J.; Schaller, R. D.; Htoon, H.; Hollingsworth, J. A. Suppressed Blinking and Auger Recombination in Near-Infrared Type-II InP/CdS Nanocrystal Quantum Dots. *Nano Lett.* **2012**, *12* (11), 5545–5551.

(81) Hao, J. J.; Zhou, J.; Zhang, C. Y. A Tri-n-Octylphosphine-Assisted Successive Ionic Layer Adsorption and Reaction Method to Synthesize Multilayered Core-Shell CdSe-ZnS Quantum Dots with Extremely High Quantum Yield. *Chem. Comm.* **2013**, *49* (57), 6346–6348.

(82) Ithurria, S.; Talapin, D. V. Colloidal Atomic Layer Deposition (c-ALD) Using Self-Limiting Reactions at Nanocrystal Surface Coupled to Phase Transfer between Polar and Nonpolar Media. *J. Am. Chem. Soc.* **2012**, *134* (45), 18585–18590.

(83) Le Monnier, B. P.; Wells, F.; Talebkeikhah, F.; Luterbacher, J. S. Atomic Layer Deposition on Dispersed Materials in Liquid Phase by Stoichiometrically Limited Injections. *Adv. Mater.* **2019**, *31* (52), 1–7.

(84) Loiudice, A.; Strach, M.; Saris, S.; Chernyshov, D.; Buonsanti, R. Universal Oxide Shell Growth Enables in Situ Structural Studies of Perovskite Nanocrystals during the Anion Exchange Reaction. *J. Am. Chem. Soc.* **2019**, *141* (20), 8254–8263.

(85) Van Huis, M. A.; Kunneman, L. T.; Overgaag, K.; Xu, Q.; Pandraud, G.; Zandbergen, H. W.; Vanmaekelbergh, D. Low-Temperature Nanocrystal Unification through Rotations and Relaxations Probed by in Situ Transmission Electron Microscopy. *Nano Lett.* **2008**, *8* (11), 3959–3963.

(86) Lambert, K.; Dendooven, J.; Detavernier, C.; Hens, Z. Embedding Quantum Dot Monolayers in Al2O3 Using Atomic Layer Deposition. *Chem. Mater.* **2011**, *23* (2), 126–128.

(87) Ihly, R.; Tolentino, J.; Liu, Y.; Gibbs, M.; Law, M. The Photothermal Stability of PbS Quantum Dot Solids. *ACS Nano* **2011**, *5* (10), 8175–8186.

(88) Liu, Y.; Gibbs, M.; Perkins, C. L.; Tolentino, J.; Zarghami, M. H.; Bustamante, J.; Law, M. Robust, Functional Nanocrystal Solids by Infilling with Atomic Layer Deposition. *Nano Lett.* **2011**, *11* (12), 5349–5355.

(89) Liu, Y.; Tolentino, J.; Gibbs, M.; Ihly, R.; Perkins, C. L.; Liu, Y.; Crawford, N.; Hemminger, J. C.; Law, M. PbSe Quantum Dot Field-Effect Transistors with Air-Stable Electron Mobilities above 7 Cm2 V-1 s-1. *Nano Lett.* **2013**, *13* (4), 1578–1587.

(90) Hu, C.; Gassenq, A.; Justo, Y.; Devloo-Casier, K.; Chen, H.; Detavernier, C.; Hens, Z.; Roelkens, G. Air-Stable Short-Wave Infrared PbS Colloidal Quantum Dot Photoconductors Passivated with Al2O3 Atomic Layer Deposition. *Appl. Phys. Lett.* **2014**, *105* (17), 3–7.

(91) Yin, B.; Sadtler, B.; Berezin, M. Y.; Thimsen, E. Quantum Dots Protected from Oxidative Attack Using Alumina Shells Synthesized by Atomic Layer Deposition. *Chem. Comm.* **2016**, *52* (74), 11127–11130.

(92) Cheng, C. Y.; Mao, M. H. Photo-Stability and Time-Resolved Photoluminescence Study of Colloidal CdSe/ZnS Quantum Dots Passivated in Al2O3 Using Atomic Layer Deposition. *J. Appl. Phys.* **2016**, *120* (8).

(93) Palei, M.; Caligiuri, V.; Kudera, S.; Krahne, R. Robust and Bright Photoluminescence from Colloidal Nanocrystal/Al2O3 Composite Films Fabricated by Atomic Layer Deposition. *ACS Appl. Mater. Interfaces* **2018**, *10* (26), 22356–22362.

(94) Bose, R.; Dangerfield, A.; Rupich, S. M.; Guo, T.; Zheng, Y.; Kwon, S.; Kim, M. J.; Gartstein, Y. N.; Esteve, A.; Chabal, Y. J.; Malko, A. V. Engineering Multilayered Nanocrystal Solids with Enhanced Optical Properties Using Metal Oxides for Photonic Applications. *ACS Appl. Nano Mater.* **2018**, *1* (12), 6782–6789.

(95) Loiudice, A.; Saris, S.; Oveisi, E.; Alexander, D. T. L.; Buonsanti, R. CsPbBr3 QD/AlOx Inorganic Nanocomposites with Exceptional Stability in Water, Light, and Heat. *Angew. Chemie* **2017**, *129* (36), 11099–11099.

(96) Crisp, R. W.; Hashemi, F. S. M.; Alkemade, J.; Kirkwood, N.; Grimaldi, G.; Kinge, S.; Siebbeles, L. D. A.; van Ommen, J. R.; Houtepen, A. J. Atomic Layer Deposition of ZnO on InP Quantum Dot Films for Charge Separation, Stabilization, and Solar Cell Formation. *Adv. Mater. Interfaces* **2020**, *7* (4), 1–8.

(97) Boles, M. A.; Ling, D.; Hyeon, T.; Talapin, D. V. The Surface Science of Nanocrystals. *Nat. Mater.* **2016**, *15*, 141–153.

(98) Jeannin, M.; Cremel, T.; Häyrynen, T.; Gregersen, N.; Bellet-Amalric, E.; Nogues, G.; Kheng, K. Enhanced Photon Extraction from a Nanowire Quantum Dot Using a Bottom-Up Photonic Shell. *Phys. Rev. Appl.* **2017**, *8* (5), 1–8.

(99) Devloo-Casier, K.; Geiregat, P.; Ludwig, K. F.; Van Stiphout, K.; Vantomme, A.; Hens, Z.; Detavernier, C.; Dendooven, J. A Case Study of ALD Encapsulation of Quantum Dots: Embedding Supported CdSe/CdS/ZnS Quantum Dots in a ZnO Matrix. *J. Phys. Chem. C* **2016**, *120* (32), 18039–18045.

(100) Kuhs, J.; Werbrouck, A.; Zawacka, N.; Drijvers, E.; Smet, P. F.; Hens, Z.; Detavernier, C. In Situ Photoluminescence of Colloidal Quantum Dots during Gas Exposure - The Role of Water and Reactive Atomic Layer Deposition

Precursors. *ACS Appl. Mater. Interfaces* **2019**, *11* (29), 26277–26287.

(101) Beard, M. C.; Luther, J. M.; Semonin, O. E.; Nozik, A. J. Third Generation Photovoltaics Based on Multiple Exciton Generation in Quantum Confined Semiconductors. *Acc. Chem. Res.* **2013**, *46* (6), 1252–1260.

(102) Ten Cate, S.; Liu, Y.; Suchand Sandeep, C. S.; Kinge, S.; Houtepen, A. J.; Savenije, T. J.; Schins, J. M.; Law, M.; Siebbeles, L. D. A. Activating Carrier Multiplication in PbSe Quantum Dot Solids by Infilling with Atomic Layer Deposition. *J. Phys. Chem. Lett.* **2013**, *4* (11), 1766–1770.

(103) So, H. M.; Choi, H.; Shim, H. C.; Lee, S. M.; Jeong, S.; Chang, W. S. Atomic Layer Deposition Effect on the Electrical Properties of Al2O3-Passivated PbS Quantum Dot Field-Effect Transistors. *Appl. Phys. Lett.* **2015**, *106* (9), 1–6.

(104) Ip, A. H.; Labelle, A. J.; Sargent, E. H. Efficient, Air-Stable Colloidal Quantum Dot Solar Cells Encapsulated Using Atomic Layer Deposition of a Nanolaminate Barrier. *Appl. Phys. Lett.* **2013**, *103* (26).

(105) Lin, C.; Tsai, F. Y.; Lee, M. H.; Lee, C. H.; Tien, T. C.; Wang, L. P.; Tsai, S. Y. Enhanced Performance of Dye-Sensitized Solar Cells by an Al2O3 Charge-Recombination Barrier Formed by Low-Temperature Atomic Layer Deposition. *J. Mater. Chem.* **2009**, *19* (19), 2999–3003.

(106) Roelofs, K. E.; Brennan, T. P.; Dominguez, J. C.; Bailie, C. D.; Margulis, G. Y.; Hoke, E. T.; McGehee, M. D.; Bent, S. F. Effect of Al2O3 Recombination Barrier Layers Deposited by Atomic Layer Deposition in Solid-State CdS Quantum Dot-Sensitized Solar Cells. *J. Phys. Chem. C* **2013**, *117* (11), 5584–5592.

(107) Saris, S.; Loiudice, A.; Mensi, M.; Buonsanti, R. Exploring Energy Transfer in a Metal/Perovskite Nanocrystal Antenna to Drive Photocatalysis. *J. Phys. Chem. Lett.* **2019**, *10* (24), 7797–7803.

(108) Federspiel, F.; Froehlicher, G.; Nasilowski, M.; Pedetti, S.; Mahmood, A.; Doudin, B.; Park, S.; Lee, J. O.; Halley, D.; Dubertret, B.; Gilliot, P.; Berciaud, S. Distance Dependence of the Energy Transfer Rate from a Single Semiconductor Nanostructure to Graphene. *Nano Lett.* **2015**, *15* (2), 1252–1258.

(109) Erdem, O.; Gungor, K.; Guzelturk, B.; Tanriover, I.; Sak, M.; Olutas, M.; Dede, D.; Kelestemur, Y.; Demir, H. V. Orientation-Controlled Nonradiative Energy Transfer to Colloidal Nanoplatelets: Engineering Dipole Orientation

Factor. *Nano Lett.* **2019**, *19* (7), 4297–4305.

(110) Guntern, Y. T.; Pankhurst, J. R.; Vávra, J.; Mensi, M.; Mantella, V.; Schouwink, P.; Buonsanti, R. Nanocrystal/Metal–Organic Framework Hybrids as Electrocatalytic Platforms for CO2 Conversion. *Angew. Chemie - Int. Ed.* **2019**, *58* (36), 12632–12639.

(111) Zhao, Y.; Kornienko, N.; Liu, Z.; Zhu, C.; Asahina, S.; Kuo, T. R.; Bao, W.; Xie, C.; Hexemer, A.; Terasaki, O.; Yang, P.; Yaghi, O. M. Mesoscopic Constructs of Ordered and Oriented Metal-Organic Frameworks on Plasmonic Silver Nanocrystals. *J. Am. Chem. Soc.* **2015**, *137* (6), 2199–2202.

(112) Fan, H. J.; Knez, M.; Scholz, R.; Nielsch, K.; Pippel, E.; Hesse, D.; Zacharias, M.; Gösele, U. Monocrystalline Spinel Nanotube Fabrication Based on the Kirkendall Effect. *Nat. Mater.* **2006**, *5* (8), 627–631.

(113) Trizio, L. De; Manna, L. Forging Colloidal Nanostructures via Cation Exchange Reactions. *Chem. Rev.* **2016**, *116*, 10852–10887.

(114) Kortan, A. R.; Hull, R.; Opila, R. L.; Bawendi, M. G.; Steigerwald, M. L.; Carroll, P. J.; Brus, L. E. Nucleation and Growth of CdSe on ZnS Quantum Crystallite Seeds, and Vice Versa, in Inverse Micelle Media. *J. Am. Chem. Soc.* **1990**, *112* (4), 1327–1332.

(115) Mews, A.; Eychmueller, A.; Giersig, M.; Schooss, D.; Weller, H. Preparation, Characterization, and Photophysics of the Quantum Dot Quantum Well System CdS/HgS/CdS. *J. Phys. Chem.* **1994**, *98* (3), 934–941.

(116) Taniguchi, S.; Green, M. The Synthesis of CdTe/ZnS Core/Shell Quantum Dots Using Molecular Single-Source Precursors. *J. Mater. Chem. C* **2015**, *3* (32), 8425–8433.

(117) Chen, D.; Zhao, F.; Qi, H.; Rutherford, M.; Peng, X. Bright and Stable Purple/Blue Emitting CdS/ZnS Core/Shell Nanocrystals Grown by Thermal Cycling Using a Single-Source Precursor. *Chem. Mater.* **2010**, *22* (4), 1437–1444.

(118) Wang, J.; Lu, Y.; Peng, F.; Zhong, Y.; Zhou, Y.; Jiang, X.; Su, Y.; He, Y. Photostable Water-Dispersible NIR-Emitting CdTe/CdS/ZnS Core-Shell-Shell Quantum Dots for High-Resolution Tumor Targeting. *Biomaterials* **2013**, *34* (37), 9509–9518.

(119) Law, W. C.; Yong, K. T.; Roy, I.; Ding, H.; Hu, R.; Zhao, W.; Prasad, P. N. Aqueous-Phase Synthesis of Highly Luminescent CdTe/ZnTe Core/Shell

Quantum Dots Optimized for Targeted Bioimaging. *Small* **2009**, *5* (11), 1302–1310.

(120) Park, J.; Dvoracek, C.; Lee, K. H.; Galloway, J. F.; Bhang, H. E. C.; Pomper, M. G.; Searson, P. C. CuInSe/ZnS Core/Shell NIR Quantum Dots for Biomedical Imaging. *Small* **2011**, *7* (22), 3148–3152.

(121) Sun, Q.; Wang, Y. A.; Li, L. S.; Wang, D.; Zhu, T.; Xu, J.; Yang, C.; Li, Y. Bright, Multicoloured Light-Emitting Diodes Based on Quantum Dots. *Nat. Photonics* **2007**, *1* (12), 717–722.

(122) Steckel, J. S.; Snee, P.; Coe-Sullivan, S.; Zimmer, J. P.; Halpert, J. E.; Anikeeva, P.; Kim, L. A.; Bulovic, V.; Bawendi, M. G. Color-Saturated Green-Emitting QD-LEDs. *Angew. Chemie - Int. Ed.* **2006**, *45* (35), 5796–5799.

(123) Klimov, V. I.; Ivanov, S. A.; Nanda, J.; Achermann, M.; Bezel, I.; McGuire, J. A.; Piryatinski, A. Single-Exciton Optical Gain in Semiconductor Nanocrystals. *Nature* **2007**, *447* (7143), 441–446.

(124) Ning, Z.; Tian, H.; Yuan, C.; Fu, Y.; Qin, H.; Sun, L.; Ågren, H. Solar Cells Sensitized with Type-II ZnSe-CdS Core/Shell Colloidal Quantum Dots. *Chem. Comm.* **2011**, *47* (5), 1536–1538.

(125) Shariati, M. R.; Samadi-Maybodi, A.; Colagar, A. H. Dual Cocatalyst Loaded Reverse Type-I Core/Shell Quantum Dots for Photocatalytic Antibacterial Applications. *J. Mater. Chem. A* **2018**, *6* (41), 20433–20443.

(126) Enache, D. I.; Edwards, J. K.; Landon, P.; Solsona-Espriu, B.; Carley, A. F.; Herzing, A. A.; Watanabe, M.; Kiely, C. J.; Knight, D. W.; Hutchings, G. J. Solvent-Free Oxidation of Primary Alcohols to Aldehydes Using Au-Pd/TiO2 Catalyst. *Science* **2006**, *311* (5759), 362–365.

(127) Varandili, S. B.; Huang, J.; Oveisi, E.; De Gregorio, G. L.; Mensi, M.; Strach, M.; Vavra, J.; Gadiyar, C.; Bhowmik, A.; Buonsanti, R. Synthesis of Cu/CeO2-x Nanocrystalline Heterodimers with Interfacial Active Sites to Promote CO2 Electroreduction. *ACS Catal.* **2019**, *9* (6), 5035–5046.

(128) Sagar, L. K.; Walravens, W.; Zhao, Q.; Vantomme, A.; Geiregat, P.; Hens, Z. PbS/CdS Core/Shell Quantum Dots by Additive, Layer-by-Layer Shell Growth. *Chem. Mater.* **2016**, *28* (19), 6953–6959.

(129) Nasilowski, M.; Nienhaus, L.; Bertram, S. N.; Bawendi, M. G. Colloidal Atomic Layer Deposition Growth of PbS/CdS Core/Shell Quantum Dots. *Chem. Comm.* **2017**, *53* (5), 869–872.

(130) Lechner, R. T.; Fritz-Popovski, G.; Yarema, M.; Heiss, W.; Hoell, A.; Schülli, T. U.; Primetzhofer, D.; Eibelhuber, M.; Paris, O. Crystal Phase Transitions in the Shell of PbS/CdS Core/Shell Nanocrystals Influences Photoluminescence Intensity. *Chem. Mater.* **2014**, *26* (20), 5914–5922.

(131) Sagar, L. K.; Walravens, W.; Maes, J.; Geiregat, P.; Hens, Z. HgSe/CdE (E = S, Se) Core/Shell Nanocrystals by Colloidal Atomic Layer Deposition. *J. Phys. Chem. C* **2017**, *121* (25), 13816–13822.

(132) Slejko, E. A.; Sayevich, V.; Cai, B.; Gaponik, N.; Lughi, V.; Lesnyak, V.; Eychmüller, A. Precise Engineering of Nanocrystal Shells via Colloidal Atomic Layer Deposition. *Chem. Mater.* **2017**, *29* (19), 8111–8118.

(133) Hazarika, A.; Fedin, I.; Hong, L.; Guo, J.; Srivastava, V.; Cho, W.; Coropceanu, I.; Portner, J.; Diroll, B. T.; Philbin, J. P.; Rabani, E.; Klie, R.; Talapin, D. V. Colloidal Atomic Layer Deposition with Stationary Reactant Phases Enables Precise Synthesis of "Digital" II-VI Nano-Heterostructures with Exquisite Control of Confinement and Strain. *J. Am. Chem. Soc.* **2019**, *141* (34), 13487–13496.

(134) Razgoniaeva, N.; Carrillo, L.; Burchfield, D.; Moroz, P.; Adhikari, P.; Yadav, P.; Khon, D.; Zamkov, M. Colloidal Synthesis of Monodisperse Semiconductor Nanocrystals through Saturated Ionic Layer Adsorption. *Chem. Mater.* **2016**, *28* (8), 2823–2833.

(135) Tessier, M. D.; Mahler, B.; Nadal, B.; Heuclin, H.; Pedetti, S.; Dubertret, B. Spectroscopy of Colloidal Semiconductor Core/Shell Nanoplatelets with High Quantum Yield. *Nano Lett.* **2013**, *13* (7), 3321–3328.

(136) Owen, J. The Coordination Chemistry of Nanocrystal Surfaces. *Science* **2015**, *347* (6222), 615–616.

(137) Hens, Z.; Martins, J. C. A Solution NMR Toolbox for Characterizing the Surface Chemistry of Colloidal Nanocrystals. *Chem. Mater.* **2013**, *25* (8), 1211–1221.

(138) Owen, J. S.; Park, J.; Trudeau, P. E.; Alivisatos, A. P. Reaction Chemistry and Ligand Exchange at Cadmium-Selenide Nanocrystal Surfaces. *J. Am. Chem. Soc.* **2008**, *130* (37), 12279–12281.

(139) Piveteau, L.; Dirin, D.; Gordon, C. P.; Walder, B. J.; Ong, T.-C.; Emsley, L.; Copéret, C.; Kovalenko, M. V. Colloidal-ALD-Grown Core/Shell CdSe/CdS Nanoplatelets as Seen by DNP Enhanced PASS-PIETA NMR Spectroscopy.

Nano Lett. **2020**, *20* (5), 3003–3018.

(140) Ithurria, S.; Tessier, M. D.; Mahler, B.; Lobo, R. P. S. M.; Dubertret, B.; Efros, A. L. Colloidal Nanoplatelets with Two-Dimensional Electronic Structure. *Nat. Mater.* **2011**, *10* (12), 936–941.

(141) Zhang, J.; Zhang, H.; Cao, W.; Pang, Z.; Li, J.; Shu, Y.; Zhu, C.; Kong, X.; Wang, L.; Peng, X. Identification of Facet-Dependent Coordination Structures of Carboxylate Ligands on CdSe Nanocrystals. *J. Am. Chem. Soc.* **2019**, *141* (39), 15675–15683.

(142) She, C.; Fedin, I.; Dolzhnikov, D. S.; Demortière, A.; Schaller, R. D.; Pelton, M.; Talapin, D. V. Low-Threshold Stimulated Emission Using Colloidal Quantum Wells. *Nano Lett.* **2014**, *14* (5), 2772–2777.

(143) Lhuillier, E.; Pedetti, S.; Ithurria, S.; Heuclin, H.; Nadal, B.; Robin, A.; Patriarche, G.; Lequeux, N.; Dubertret, B. Electrolyte-Gated Field Effect Transistor to Probe the Surface Defects and Morphology in Films of Thick CdSe Colloidal Nanoplatelets. *ACS Nano* **2014**, *8* (4), 3813–3820.

(144) Loiudice, A.; Saris, S.; Buonsanti, R. Tunable Metal Oxide Shell as a Spacer to Study Energy Transfer in Semiconductor Nanocrystals. *J. Phys. Chem. Lett.* **2020**, 3430–3435.

(145) Cremers, V.; Puurunen, R. L.; Dendooven, J. Conformality in Atomic Layer Deposition: Current Status Overview of Analysis and Modelling. *Appl. Phys. Rev.* **2019**, *6* (2), 021302.

(146) Cameron, M. A.; Gartland, I. P.; Smith, J. A.; Diaz, S. F.; George, S. M. Atomic Layer Deposition of SiO2 and TiO2 in Alumina Tubular Membranes: Pore Reduction and Effect of Surface Species on Gas Transport. *Langmuir* **2000**, *16* (19), 7435–7444.

(147) Dendooven, J.; Devloo-Casier, K.; Ide, M.; Grandfield, K.; Kurttepeli, M.; Ludwig, K. F.; Bals, S.; Van Der Voort, P.; Detavernier, C. Atomic Layer Deposition-Based Tuning of the Pore Size in Mesoporous Thin Films Studied by in Situ Grazing Incidence Small Angle X-Ray Scattering. *Nanoscale* **2014**, *6* (24), 14991–14998.

(148) Saris, S.; Dona, S. T.; Niemann, V.; Loiudice, A.; Buonsanti, R. Optimizing the Atomic Layer Deposition of Alumina on Perovskite Nanocrystal Films by Using O2 As a Molecular Probe. *Helv. Chim. Acta* **2020**, *103*, e2000055.

(149) Valdesueiro, D.; Prabhu, M. K.; Guerra-Nunez, C.; Sandeep, C. S. S.; Kinge,

S.; Siebbeles, L. D. A.; De Smet, L. C. P. M.; Meesters, G. M. H.; Kreutzer, M. T.; Houtepen, A. J.; Van Ommen, J. R. Deposition Mechanism of Aluminum Oxide on Quantum Dot Films at Atmospheric Pressure and Room Temperature. *J. Phys. Chem. C* **2016**, *120* (8), 4266–4275.

(150) Poodt, P.; Cameron, D. C.; Dickey, E.; George, S. M.; Kuznetsov, V.; Parsons, G. N.; Roozeboom, F.; Sundaram, G.; Vermeer, A. Spatial Atomic Layer Deposition: A Route towards Further Industrialization of Atomic Layer Deposition. *J. Vac. Sci. Technol. A* **2012**, *30* (1), 010802.

(151) Miikkulainen, V.; Leskelä, M.; Ritala, M.; Puurunen, R. L. Crystallinity of Inorganic Films Grown by Atomic Layer Deposition: Overview and General Trends. *J. Appl. Phys.* **2013**, *113* (2).

(152) Li, G.; Rivarola, F. W. R.; Davis, N. J. L. K.; Bai, S.; Jellicoe, T. C.; De La Peña, F.; Hou, S.; Ducati, C.; Gao, F.; Friend, R. H.; Greenham, N. C.; Tan, Z. K. Highly Efficient Perovskite Nanocrystal Light-Emitting Diodes Enabled by a Universal Crosslinking Method. *Adv. Mater.* **2016**, *28* (18), 3528–3534.